Atmos. Chem. Phys., 18, 12011–12044, 2018
https://doi.org/10.5194/acp-18-12011-2018

Atmospheric Chemistry and Physics
Open Access
EGU

A comparison of posterior atmospheric CO_2 adjustments obtained from in situ and GOSAT constrained flux inversions

Saroja M. Polavarapu[1], **Feng Deng**[2], **Brendan Byrne**[2], **Dylan B. A. Jones**[2], **and Michael Neish**[1]

[1]Climate Research Division, Environment and Climate Change Canada, Toronto, Ontario, M3H 5T4, Canada
[2]Dept. of Physics, University of Toronto, Toronto, Ontario, M5S 1A7, Canada

Correspondence: Saroja M. Polavarapu (saroja.polavarapu@canada.ca)

Received: 29 December 2017 – Discussion started: 10 January 2018
Revised: 6 July 2018 – Accepted: 25 July 2018 – Published: 22 August 2018

Abstract. Posterior fluxes obtained from inverse modelling are difficult to verify because there is no dense network of flux measurements available to evaluate estimates against. Here we present a new diagnostic to evaluate structures in posterior fluxes. First, we simulate the change in atmospheric CO_2 fields between posterior and prior fluxes, referred to as the posterior atmospheric adjustments due to updated fluxes (PAAFs). Second, we calculate the uncertainty in atmospheric CO_2 fields due solely to uncertainty in the meteorological fields, referred to as the posterior atmospheric adjustments due to imperfect meteorology (PAAMs). We argue that PAAF can only be considered robust if it exceeds PAAM, that is, the changes in atmospheric CO_2 between the posterior and prior fluxes should at least exceed atmospheric CO_2 changes arising from imperfect meteorology. This diagnostic is applied to two CO_2 flux inversions: one which assimilates observations from the in situ CO_2 network and the other which assimilates observations from the Greenhouse Gases Observing SATellite (GOSAT). On the global scale, PAAF in the troposphere reflects northern extratropical fluxes, whereas stratospheric adjustments primarily reflect tropical fluxes. In general, larger spatiotemporal variations in PAAF are obtained for the GOSAT inversion than for the in situ inversion. Zonal standard deviations of the PAAF exceed the PAAM through most of the year when GOSAT observations are used, but the minimum value is exceeded only in boreal summer when in situ observations are used. Zonal spatial structures in GOSAT-based PAAF exceed PAAM throughout the year in the tropics and through most of the year in the northern extratropics, suggesting GOSAT flux inversions can constrain zonal asymmetries in fluxes. However, we cannot discount the possibility that these structures are influenced by biases in GOSAT retrievals. Verification of such spatial structures will require a dense network of independent observations. Because PAAF depends on the choice of prior fluxes, the comparison with PAAM is system dependent and thus can be used to monitor a given assimilation system's behaviour.

1 Introduction

Flux inversion systems have become useful tools for understanding the global carbon budget, as evidenced by their presence in Intergovernmental Panel on Climate Change (IPCC) reports (Ciais et al., 2013). However, even with the expansion of the near-surface in situ network, limitations remain in the ability to retrieve regional-scale fluxes (Bruhwiler et al., 2011). Thus, with the promise of retrieving fluxes with higher spatial resolution, the first satellite missions dedicated to greenhouse gas measurements from space were launched: the Greenhouse Gases Observing SATellite (GOSAT) in 2009 (Kuze et al., 2009) and the Orbiting Carbon Observatory (OCO-2) (Crisp and OCO-2 Science Team, 2015; Crisp et al., 2017) in 2014. The expec-

tation was that not only should space-based measurements of column-integrated CO_2 offer better spatial coverage, but the column amount should be less sensitive to modelling errors associated with the planetary boundary layer (PBL) and its representativeness should better correspond to that of coarse model grids (Keppel-Aleks et al., 2011). This occurs because mainly long-range fluxes are seen in column data, whereas both local and long-range flux signals are seen by surface in situ observations (Keppel-Aleks et al., 2011). Thus, space-based measurements of column-integrated CO_2 offered the promise of alleviating some of the challenges associated with the assimilation of near-surface in situ measurements in flux inversion systems. However, that promise has yet to be realized. Regional flux estimates have not been robust (e.g. Maksyutov et al., 2013; Basu et al., 2013; Chevallier et al., 2014; Deng et al., 2014; Houweling et al., 2015) and they are sensitive to biases in satellite retrievals (Basu et al., 2013; Deng et al., 2014; Takagi et al., 2014). Retrieved uptake by the European biosphere is twice as large in GOSAT inversions compared to in situ inversions (Reuter et al., 2014, 2017), with many studies finding such increased sinks (Houweling et al., 2015; Feng et al., 2016). It has been suggested that the GOSAT-based inversions shift some uptake from northern Africa to Europe, which reduces the north–south gradient in CO_2 and reduces agreement with observations (Houweling et al., 2015). The issue may also be due to the impact of non-local observations in flux inversion systems since biases in upstream CO_2 contribute 60 %–90 % of the European sink (Feng et al., 2016). However, the uneven spatial coverage of the in situ network may also be playing a role in the discrepancy. Bruhwiler et al. (2011) found that the inclusion of newer European sites results in a large rebalancing of uptake from Europe to boreal Eurasia in comparison to an inversion with existing older sites. Kim et al. (2017) found that after adding Siberian in situ measurements to their inversion system, the carbon uptake in Europe was enhanced while it decreased in the Eurasian boreal TransCom region. The point is that within the context of flux inversion systems, this new type of measurement poses new challenges. These challenges are related to aspects of the data specific to satellite column measurements. For example, biases arise from sampling only clear skies (Corbin et al., 2009; Parazoo et al., 2012) and from the seasonal variation of observational coverage (Liu et al., 2014; Byrne et al., 2017). At the same time, model transport errors remain an issue for inversions using column measurements. Model errors in simulating boundary layer mixing are still important for assimilating column measurements (Lauvaux and Davis, 2014), isentropic transport needs to be correctly modelled (Parazoo et al., 2012; Barnes et al., 2016) and model biases in the high latitude upper troposphere can impact the north–south distribution of fluxes (Deng et al., 2015). Thus, it is important to get not only the low-level vertical gradients correct in the transport model, but also the upper tropospheric and lower stratospheric distributions that the satellites are sensitive to. Ultimately, the best network will combine surface and satellite measurements (Baker et al., 2006; Basu et al., 2013; Lauvaux and Davis, 2014). The question is how to use the different types of observations to their strengths within a given data assimilation system.

The goal of this work is to improve our understanding of how the different types of CO_2 observing systems can inform model simulations of CO_2 by (1) examining the imprint of inversion flux corrections in atmospheric CO_2 and (2) determining if this imprint is larger than CO_2 changes that arise solely from meteorological uncertainties. The imprint of flux corrections in atmospheric CO_2 can be found by simulating the change in atmospheric CO_2 fields between posterior and prior fluxes, which we refer to as the posterior atmospheric adjustments (PAAs) due to updated fluxes (PAAFs).

The PAAF assumes that the meteorological fields are known exactly. However, there are known to be significant uncertainties in meteorological fields. For instance, Liu et al. (2011) estimate the uncertainty due to meteorology as 1.2–3.5 ppm at the surface and 0.8–1.8 ppm in a column mean CO_2 fields. This level of uncertainty can be calculated using an online weather and greenhouse gases transport model. Meteorological observations can be assimilated into the analysis to produce an error estimate in atmospheric transport (using an ensemble Kalman filter in our set-up). From this error estimate one can quantify a minimum level of uncertainty in CO_2 distributions arising from imperfect knowledge of wind fields, referred to as posterior atmospheric adjustments due to imperfect meteorology (PAAMs). If PAAF is larger than PAAM it implies that the change in atmospheric CO_2 is robust against uncertainties in meteorological fields. Thus, we argue that atmospheric CO_2 adjustments due to retrieved fluxes should at least exceed the minimum level of uncertainty in CO_2 distributions arising from imperfect knowledge of wind fields in order for the retrieved fluxes to be considered robust against transport errors. Since PAAF depends on the choice of prior flux, a better prior flux would yield a smaller PAAF because the observations have less to correct for during the flux inversion. Thus, the diagnostic is system dependent, but this means it would be useful for monitoring improvements in prior fluxes and model transport. It can also be used to identify when meteorological errors become the limiting factor to improving flux estimates.

To illustrate the utility of this new diagnostic, we compare the 3-D structure of the (PAAFs) estimated from the in situ observing network and from GOSAT. Because satellite data are sensitive to the full column of CO_2 concentrations, accurate forward model simulations throughout the troposphere and lower stratosphere are needed in order to be able to correctly attribute model–data mismatch to upstream surface fluxes. Thus, we focus on assessing posterior CO_2 distributions at various heights by comparing to observations. In addition, the spatio-temporal evolution of the PAAFs is examined through its global mean evolution, zonal mean structures and zonal asymmetries. Two different tracer trans-

port models, GEOS-Chem (http://geos-chem.org, last access: 7 August 2018) and GEM-MACH-GHG (Polavarapu et al., 2016), are used to simulate the propagation of the PAAF. This allows an investigation of the sensitivity of our results to transport errors between the models. Furthermore, since GEM-MACH-GHG is a coupled weather and greenhouse gas (GHG) transport model, we are able to determine uncertainties in our diagnostics that arise due to imperfections in meteorological analyses (PAAM). Only when PAAF diagnostics exceed such minimum uncertainty levels do we find potential benefits of a given observing system.

The article is organized as follows. The experimental design is presented in Sect. 2. Here the observations used for assimilation and verification, the transport models and the flux inversion system, are all described. Section 3 presents the results. First the posterior fluxes are briefly compared (Sect. 3.1) before the impact of posterior fluxes on CO_2 distributions is examined (Sect. 3.2). Diagnostics focus on variations of the PAAF on global scales and in three zonal bands. Because PAAF cannot be directly verified, comparisons to independent observations of CO_2 are also made, to inform the discussions of PAAF differences due to the different observing systems. Section 4 summarizes the results and considers their implications and generality.

2 The experimental design

In order to understand how the PAAF retrieved from assimilating atmospheric observations propagates into the vertical, we must first perform some flux inversions. There are two sets of flux inversions performed with the GEOS-Chem model and these are based on either the in situ observation network or on GOSAT column measurements. In order to assess the quality of the CO_2 distributions from the two observing systems, we compare posterior CO_2 distributions to independent measurements that contain some information about the vertical distribution of CO_2, namely, aircraft profiles from measurement campaigns, routine NOAA aircraft profiles and the ground-based column measurement network. These comparisons will inform subsequent discussions of PAAF. Section 2.1 describes the observation systems used in the flux inversions as well as those used for validation of modelled CO_2 distributions. The models used are presented in Sect. 2.2. The posterior atmospheric adjustment and its components (PAAF, PAAM) are defined mathematically in Sect. 2.3 while Sect. 2.4 explains how they are computed.

2.1 The observations

The in situ observation network primarily consists of CO_2 mixing ratios measured by a nondispersive infrared absorption technique applied to air samples collected in glass flasks at the NOAA ESRL Carbon Cycle Cooperative Global Air Sampling Network sites (Conway et al., 2011) and at the Environment and Climate Change Canada (ECCC) sampling sites. We use the same 72 NOAA sites and 6 ECCC sites that were used by Deng et al. (2014). Figure 1 shows the approximate distribution of the in situ observations, as well as the validating observations (described below). Since observing stations may have missing data or may start or stop during the period of interest, the figure is only meant to provide a general idea of the spatial distribution of the in situ observation network. While the coverage is global, the density of the stations is sparse, particularly in the tropics and Southern Hemisphere. However, the measurements are accurate, to better than 0.2 ppm (Tans and Thoning, 2016). The CO_2 measurements reflect the influence of local as well as remote sources (Keppel-Aleks et al., 2012; Byrne et al., 2017).

The satellite data used this paper are version b3.4 of the NASA Atmospheric CO_2 Observations from Space (ACOS) GOSAT XCO_2 product, spanning July 2009 to December 2011, and have been bias-corrected (Osterman et al., 2013). The ACOS retrievals employ an optimal estimation approach to infer atmospheric profile abundances of CO_2, from which XCO_2 is calculated. The details of the retrieval are described in O'Dell et al. (2012). Takagi et al. (2014) and Deng et al. (2014) showed that the biases of different versions of GOSAT products impact regional flux estimates but Deng et al. (2016) found that fluxes from version b3.4 result in CO_2 distributions that compare well to independent measurements. Hence, the XCO_2 data used here are exactly those used in Deng et al. (2016). In addition, Deng et al. (2016) found that assimilating ocean glint measurements in addition to land nadir measurements results in generally improved agreement with independent observations and so both types of GOSAT data are also used here. Figure 2 shows that, in contrast to the fixed locations of the ground-based in situ observations, satellite observations have a seasonal variation. In particular, in boreal summer when CO_2 uptake by the terrestrial biosphere in the Northern Hemisphere dominates the global CO_2 evolution, observations are dense. In austral summer, the satellite's observational coverage shifts southward and the southern mid-latitudes are observed well. Throughout the year, ocean glint measurements observe the tropical oceans and improve the estimation of tropical fluxes (Deng et al., 2016).

Since posterior atmospheric adjustments are not directly verifiable, the impact of the inversion results on CO_2 distributions are evaluated by comparing posterior CO_2 fields with atmospheric CO_2 observations from the Total Carbon Column Observing Network (TCCON) (https://tccondata.org, last access: 7 August 2018) (Wunch et al., 2011). At the TCCON sites, solar-viewing ground-based Fourier transform spectrometers are used to measure high-resolution spectra ($0.02\,cm^{-1}$) in the near-infrared range ($3800–15\,500\,cm^{-1}$), from which XCO_2 is retrieved. For the comparisons, we use observations from the current TCCON GGG2014 data set from 14 different sites (Blumenstock et al., 2014; Deutscher et al., 2014; Griffith et al., 2014a, b; Hase et al., 2014; Kivi et

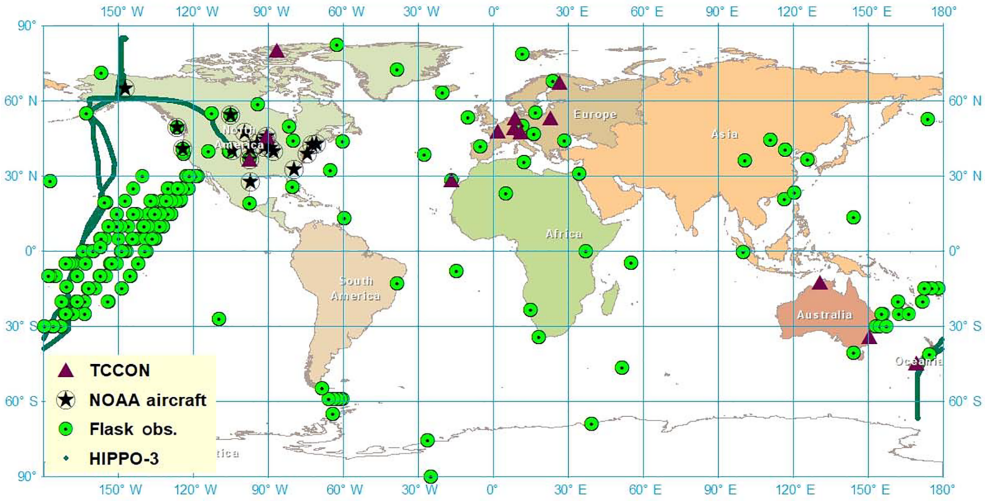

Figure 1. In situ observation network and observations used for verification. The in situ observations used in the GEOS-Chem flux inversion are indicated in green circles. Observations used for model assessment are also shown: TCCON (triangles), NOAA aircraft (stars) and HIPPO-3 aircraft (green line).

al., 2014; Notholt et al., 2014; Sherlock et al., 2014; Strong et al., 2014; Sussmann and Rettinger 2014; Warneke et al., 2014; Wennberg et al., 2014a, b). While total column measurements can indicate the quality of modelled CO_2 simulations throughout the troposphere, they do not provide information on vertical distributions. For a more direct indication of model performance in the middle and upper troposphere, we also evaluate the inversions using aircraft data from the HIAPER Pole-to-Pole Observations (HIPPO) aircraft campaign (http://hippo.ornl.gov/, last access: 7 August 2018) as well as NOAA aircraft profiles (Sweeney et al., 2015). Specifically, the 10 s averaged data from the HIPPO-3 campaign (Wofsy et al., 2012, 2011) are used for 24 March to 16 April 2010. The NOAA aircraft profiles were limited to flights over Canada and the continental US during 2010. The model comparisons to TCCON, HIPPO and NOAA aircraft profiles will be used to inform the discussions of posterior atmospheric adjustments in Sect. 3.

2.2 The models

2.2.1 The GEOS-Chem inversion system

The GEOS-Chem 4-dimensional variational (4D-Var) data assimilation system was used to estimate global regional CO_2 fluxes. The GEOS-Chem global 3-dimensional chemical transport model is driven by assimilated meteorological observations from the Goddard Earth Observing System (GEOS-5) of the NASA Global Modeling Assimilation Office (GMAO). The model configuration is the same as that used in Deng et al. (2014). The horizontal resolution of the model is $4° \times 5°$, with 47 vertical levels extending from the surface to 0.01 hPa. The prior CO_2 fluxes, as described in Deng et al. (2014), include CO_2 fluxes from fossil fuel combustion and cement production from the Carbon Dioxide Information Analysis Center (CDIAC) (Andres et al., 2011), monthly mean shipping emissions of CO_2 from the International Comprehensive Ocean-Atmosphere Data Set (ICOADS) (Corbett, 2004; Corbett and Koehler, 2003; Endresen et al., 2004; Endresen et al., 2007), 3-D aviation CO_2 emissions (Friedl, 1997; Kim et al., 2007; Wilkerson et al., 2010), a climatology of monthly mean ocean–atmosphere CO_2 flux by Takahashi et al. (2009), biofuel CO_2 emission based on Yevich and Logan (2003), and monthly mean biomass burning CO_2 emissions from the Global Fire Emissions Database version 3 (GFEDv3) from van der Werf et al. (2010). The model includes 3-hourly Terrestrial ecosystem exchange from the Boreal Ecosystem Productivity Simulator (BEPS) (Chen et al., 2012), which was driven by NCEP reanalysis data (Kalnay et al., 1996) and remotely sensed leaf area index (LAI) (Deng et al., 2006). The annual terrestrial ecosystem exchange imposed in each grid box is neutral (Deng and Chen, 2011).

Two sets of inversions were performed using the two different observing networks for the 1 July 2009 to 30 June 2011 period (Fig. 3). The first 6 months are treated as a spin-up period and we mainly consider the estimated fluxes for January 2010–July 2011. The initial 3-D CO_2 mixing ratio fields were generated by running the model from January 1996 to December 2007 without assimilating any data, and then by assimilating surface CO_2 flask data from January 2008 to July 2010, following Deng et al. (2014). The optimized CO_2 mixing ratio field at 00:00 UTC on 1 July 2009 was used as the initial CO_2 field for the inversion analysis. As described in Deng et al. (2014), in assimilating the GOSAT data the model is transformed using the averaging kernels and prior CO_2 profiles from the XCO_2 retrievals. The as-

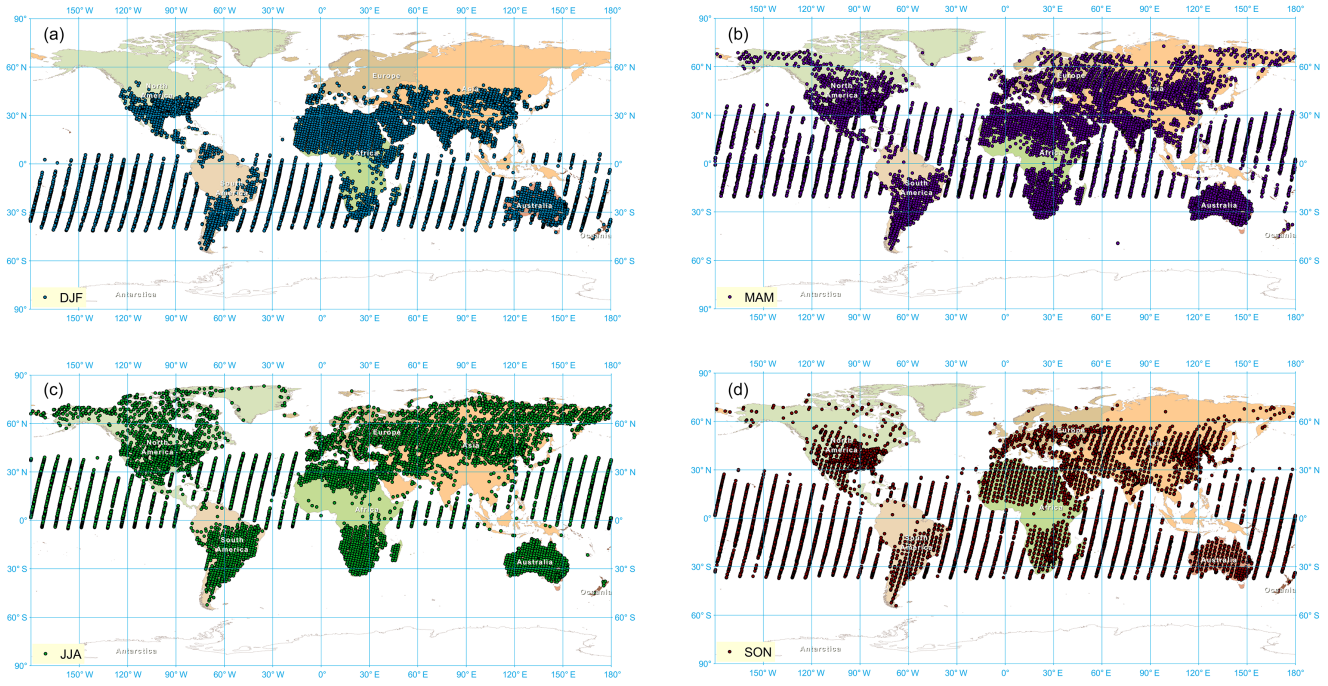

Figure 2. Seasonal variation of GOSAT observations. The observations used in the GOSAT-based flux inversions are shown for four seasons: boreal winter (December, January, February – **a**), boreal spring (March, April, May – **b**), boreal summer (June, July, August – **c**) and boreal autumn (September, October, November – **d**) for 2010.

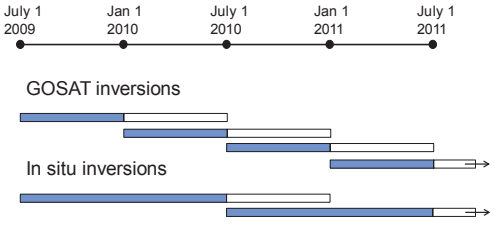

Figure 3. Schematic diagram of GEOS-Chem inversion experiments. The inversions involving the assimilation of GOSAT data were done in four 12-month segments. The fluxes obtained from the first 6 months of each segment were retained as the retrieved fluxes. The inversions involving in situ data were done in two 18-month segments with the fluxes retained from the first 12 months. Thus, retrieved fluxes were available for the 24 months from 1 July 2009 to 30 June 2011 for both sets of flux inversions.

similation did not account for horizontal correlations in the observation and prior error covariance matrices. The uncertainties applied to the GOSAT and in situ data are the same as in Deng et al. (2016, 2014), respectively. Specifically, the reported XCO_2 retrieval uncertainties were inflated by 1.90 over land and 1.02 over ocean. Uncertainties applied to in situ data were determined from model-observation statistics for each site. Prior flux uncertainties are 16 % of fossil fuel emissions and 38 % of biomass burning per grid box per month. An uncertainty of 44 % is assumed for the ocean flux and a 22 % uncertainty is assigned to both the gross primary production and total ecosystem respiration per 3 h per grid box. Detailed explanations for these choices are found in Deng et al. (2014, 2016). Each set of inversions used a different assimilation window: 18 months for the in situ network but 12 months for the GOSAT network. This difference is necessitated by the different data densities. With the sparse in situ network, sufficient time is needed to collect enough observations to determine upstream fluxes; therefore, we use an 18-month window as in Deng et al. (2014). However, with the more dense GOSAT observations (Fig. 2), flux perturbations have a greater chance of being observed quickly after injection into the atmosphere, so a shorter window will suffice. Thus, we used a 12-month assimilation window for the GOSAT inversion, as in Deng et al. (2016). Differences in the two inversion setups are inevitable because some parameters must necessarily differ (such as observation and representativeness error variances for the two measurement types). So, choosing exactly the same setup for both would force one system (and observation network) to be unfairly disadvantaged. Moreover, our intention is to examine the fluxes retrieved from what we believe to be the "best" configuration for each.

2.2.2 The GEM-MACH-GHG model

GEM-MACH-GHG is a global, coupled weather and greenhouse gas prediction model with approximately 0.9° horizontal grid spacing and 80 vertical levels spanning the ground to

the mesosphere (0.01 hPa). It is derived from the operational weather forecast model used for global and regional predictions by the Canadian Meteorological Centre and is described in detail in Polavarapu et al. (2016). A semi-Lagrangian advection scheme is used for meteorology and constituent transport. For the latter, a global mass fixer was implemented. Convective transport of tracers through the deep convection scheme of Kain and Fritsch (Kain and Fritsch, 1990; Kain, 2004) was also implemented. The same initial condition used by GEOS-Chem was regridded to GEM-MACH-GHG's grid. Because of the large differences in model resolution and topography, the global air masses in the two models differ so forcing mass conservation during the regridding process introduced local differences in mixing ratios. In particular, the GEM-MACH-GHG initial condition has a bias of about 0.5 ppm in the Southern Hemisphere. Since all model integrations use the same initial conditions, diagnostics involving a difference in model integrations (Sect. 2.3) are not affected by the initial state differences between the two models. The posterior fluxes from the GEOS-Chem assimilation are inserted every model time step with 3 h updates. Note that posterior fluxes contain the total of all optimized (GPP, respiration, ocean, biomass burning and anthropogenic) fluxes and the small amount of un-optimized fossil fuel emissions from shipping ($\sim 0.19\,\mathrm{Pg\,C\,yr^{-1}}$) and aviation ($\sim 0.16\,\mathrm{Pg\,C\,yr^{-1}}$). Since GEM-MACH-GHG does not yet have the ability to insert 3-dimensional emissions as GEOS-Chem does, the aircraft emissions were not inserted. This will lead to an underestimate in global CO_2 of less than $0.1\,\mathrm{ppm\,yr^{-1}}$.

2.3 The posterior atmospheric adjustment

In this section, we introduce a new diagnostic for flux inversion results. To do this, we first mathematically define the posterior atmospheric adjustment and show that, in general, it is comprised of a number of components. In our work, we will compute two of these components: the component due to flux adjustments and that due to meteorological uncertainty. By comparing these two components we can determine which is the dominant one. In particular, we are interested in identifying when changes in CO_2 fields introduced by flux analysis increments exceed CO_2 changes obtained from random perturbations on the size and shape of meteorological analysis errors. When this does not occur, CO_2 adjustments due to fluxes are smaller than those due to transport error and are therefore not robust against transport error.

Consider a transport model:

$$c_n = T\left(x_{0,n-1}, c_0, s_{0,n-1}\right), \tag{1}$$

where T is the transport model which evolves the constituent (c) from time step 0 to time step n and which depends on the meteorological states, $x_{0,n-1}$; the constituent initial condition, c_0; and the fluxes, $s_{0,n-1}$. This same transport model is integrated twice: once with a set of prior fluxes, $s^{\mathrm{b}}_{0,n-1}$, and a second time with the posterior fluxes, $s^{\mathrm{a}}_{0,n-1}$. The posterior fluxes are related to the prior fluxes as follows:

$$s^{\mathrm{a}}_{0,n-1} = s^{\mathrm{b}}_{0,n-1} + \Delta s_{0,n-1}. \tag{2}$$

The second term on the right side is the flux increment obtained from inverse modelling, and its spatial structure strongly depends on the observations used within the inversion model. The posterior atmospheric adjustment (Δc_n) can be defined as follows:

$$\Delta c_n = T\left(x^{\mathrm{a}}_{0,n-1}, c^{\mathrm{a}}_0, s^{\mathrm{a}}_{0,n-1}\right) - T\left(x^{\mathrm{b}}_{0,n-1}, c^{\mathrm{b}}_0, s^{\mathrm{b}}_{0,n-1}\right). \tag{3}$$

The superscript "a" in Eq. (3) denotes the "after adjustment" value and the superscript "b" refers to the "before adjustment" value. This is a general form which allows for the initial state of the constituent and the meteorological states to change when the posterior flux changes (i.e. uncertainty in initial conditions and meteorology is permitted). If the initial state of the constituent is not adjusted in the flux inversion (as in our case), we can drop the superscripts on c_0. However, let us retain the possibility of meteorological analysis uncertainty where

$$x^{\mathrm{a}}_{0,n-1} = x^{\mathrm{b}}_{0,n-1} + \varepsilon_{0,n-1}. \tag{4}$$

The second term on the right side in Eq. (4) is a realization of meteorological analysis error. If a meteorological data assimilation system computes analysis error covariances, such an estimate of uncertainty can be obtained. Then, as in Polavarapu et al. (2016), we expand the transport terms in Taylor series about the posterior state as follows:

$$\begin{aligned}\Delta c_n = {} & \frac{\partial T}{\partial s}\left(x^{\mathrm{a}}_{0,n-1}, c_0, s^{\mathrm{a}}_{0,n-1}\right)\Delta s_{0,n-1} \\ & + \frac{\partial T}{\partial x}\left(x^{\mathrm{a}}_{0,n-1}, c_0, s^{\mathrm{a}}_{0,n-1}\right)\varepsilon_{0,n-1} \\ & + O\left(\Delta s_{0,n-1}\varepsilon_{0,n-1}\right).\end{aligned} \tag{5}$$

To first order, the PAA is comprised of two components (because in this work we do not consider the components of PAA related to imperfect initial concentrations):

$$\Delta c_n \cong \Delta c^s_n + \Delta c^x_n. \tag{6}$$

Table 1. Comparable model levels used in later figures. An approximate pressure level is computed for each model level assuming a reference surface pressure of 1000 hPa.

Reference pressure (hPa)	GEOS-Chem Model-level ref.		GEM Model-level ref.	
	index	hPa	index	hPa
850	9	856.781	69	854.893
500	22	503.795	57	501.327
250	28	263.587	47	258.932
100	34	99.191	34	99.1268
33	38	33.814	19	32.9691
7	41	6.588	10	6.86514

Note that for a given set of meteorological analyses, the transport model is a linear function of the flux and the linearized model is then the same as the original transport model in Eq. (5). We can approximate the components of the PAA using finite differences:

$$\Delta c_n^s = T\left(x^{\mathrm{a}}_{0,n-1}, c_0,\ s^{\mathrm{a}}_{0,n-1}\right) - T\left(x^{\mathrm{a}}_{0,n-1},\ c_0,\ s^{\mathrm{b}}_{0,n-1}\right) = \mathrm{PAAF}, \quad (7)$$

$$\Delta c_n^x = T\left(x^{\mathrm{a}}_{0,n-1}, c_0,\ s^{\mathrm{a}}_{0,n-1}\right) - T\left(x^{\mathrm{b}}_{0,n-1},\ c_0,\ s^{\mathrm{a}}_{0,n-1}\right) = \mathrm{PAAM}. \quad (8)$$

PAAF is the component of PAA due to flux adjustments while PAAM is the component of PAA due to uncertain meteorology. PAAF is computed by integrating the transport model with a set of posterior fluxes and again with the prior fluxes, but both integrations use the same set of meteorological analyses ($x^{\mathrm{a}}_{0,n-1}$) and initial concentrations. However, this is only one component of the posterior flux adjustment because the meteorological analyses are not perfectly known, and we can simulate that uncertainty by perturbing the meteorological analyses with realizations of meteorological analysis error (see Supplement for a detailed description of how this was done). In other words, for a given set of fluxes, the meteorological fields could have been slightly different but equally valid in the context of the meteorological analysis errors. This is what PAAM defines and it is computed by integrating the model twice (with perturbed and unperturbed meteorology) for a given set of posterior fluxes and where we again use the same initial concentrations in both integrations. Figure 4 illustrates these concepts schematically. Note that the impact of the meteorological uncertainty on posterior distributions is a different matter from transport biases that result from biased meteorology. The latter will be present in PAAF when it is computed with a single set of analyses but the former requires PAAM to be computed with two or more sets of analyses. A novel aspect of our work is the ability to compare the component of posterior atmospheric adjustment due to flux increments with that due to meteorological uncertainty. If the PAA component due to flux increments alone (PAAF) does not exceed the component due to meteorological errors (PAAM), then it may not be the dominant contribution in Eq. (5) and therefore it should not be accorded much significance. In reality, the story will be complex because the PAA is a 4-dimensional field and the dominant component will likely be a function temporal and spatial scale. Therefore, in what follows, we consider some broad statistics of the PAA and its subcomponents such as global means and zonal means and zonal standard deviations.

2.4 Computing contributions to posterior atmospheric adjustments

Once the flux estimates have been obtained, they are inserted into a forecast model to obtain posterior CO_2 distributions.

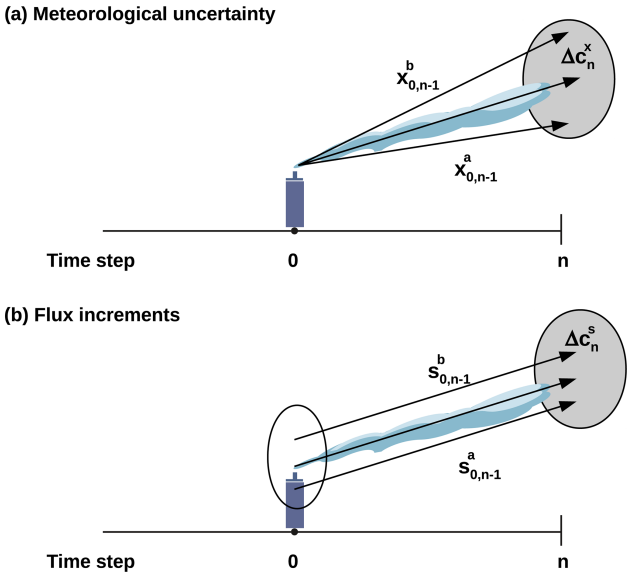

Figure 4. Components of the posterior atmospheric adjustment. **(a)** The top panel is a schematic diagram illustrating the fact that uncertain wind fields (represented by the 3 arrows) would lead to a cloud of equally plausible downstream locations for a given sequence of fluxes. **(b)** The lower panel is a schematic diagram illustrating the fact that flux increments (e.g. a prior versus a posterior flux) will lead to differences in concentrations downstream, for a given sequence of meteorological analyses. The parallel arrows are meant to indicate the use of the same meteorological fields for two flux estimates.

Prior CO_2 distributions are also obtained by inserting prior fluxes into the same model, and then the PAAF is determined by subtracting the prior CO_2 distribution from the posterior CO_2 distribution. Both model integrations use the same CO_2 initial states and meteorological fields. Here we use GEOS-Chem as well as GEM-MACH-GHG (Polavarapu et al., 2016) for this purpose. The advantage of using two models is that we can get a sense of the robustness of the results since the models will have different model errors. The disadvantage of using a different model (from that used for the flux inversions) to obtain the PAAF is that posterior fluxes contain an imprint of transport model errors from the model used for the flux inversion, so integrating these into another model will convolve the two transport models' errors (as seen in Polavarapu et al., 2016). If the two models' transport errors are fortuitously similar, then this problem is avoided. However, this is unlikely to be the case for any two models on all time and spatial scales. Thus, we assess the ability of GEM-MACH-GHG to simulate CO_2 with fluxes derived from inversions performed with GEOS-Chem in order to identify where convolution of the two transport models' errors is evident.

By comparing CO_2 distributions from GEM-MACH-GHG obtained with posterior fluxes from GEOS-Chem with observations, we can assess the ability of this model to simu-

Table 2. Comparison of GEOS-Chem and GEM-MACH-GHG CO_2 to NOAA or ECCC continuous in situ observations. The 6-season averaged seasonal means and standard deviations from Fig. 4 are given. Each box with statistics contains two numbers: the seasonal mean (left) and the standard deviation (right). Results from four experiments are shown. Two models (GEOS-Chem and GEM-MACH-GHG) were used to integrate posterior fluxes from GEOS-Chem inversions using only in situ or GOSAT observations. Units are parts per million (ppm). Note that all observations (including night-time) were used.

Alert												
	DJF 2010		MAM 2010		JJA 2010		SON 2010		DJF 2011		MAM 2011	
GEOS-Chem GOSAT	0.59	1.46	0.84	0.83	−0.02	0.96	0.58	1.08	0.13	1.48	1.11	1.03
GEOS-Chem in situ	−0.56	1.45	−0.16	0.88	1.14	0.90	−0.03	1.08	−1.09	1.46	0.20	1.07
GEM GOSAT	0.01	0.97	1.11	0.81	0.89	1.26	−0.84	0.80	−0.57	1.09	0.78	1.04
GEM in situ	−0.96	0.95	0.12	0.88	2.33	1.27	−0.96	0.79	−1.70	1.08	−0.13	1.14
No. obs.	2157		2195		2104		2079		2084		2145	
Mauna Loa												
	DJF 2010		MAM 2010		JJA 2010		SON 2010		DJF 2011		MAM 2011	
GEOS-Chem GOSAT	0.80	0.95	1.57	0.80	−0.67	1.45	−0.09	1.07	0.72	0.72	1.61	1.10
GEOS-Chem in situ	−0.14	0.91	0.54	0.78	−0.48	1.03	0.05	0.72	0.19	0.65	0.82	1.05
GEM GOSAT	1.17	0.99	1.41	0.90	−0.84	1.67	0.08	1.31	0.94	0.77	1.64	1.10
GEM in situ	0.22	0.98	0.45	0.89	−0.57	1.28	0.15	0.94	0.32	0.68	1.00	1.08
No. obs.	743		759		870		1011		994		879	
Sable Island												
	DJF 2010		MAM 2010		JJA 2010		SON 2010		DJF 2011		MAM 2011	
GEOS-Chem GOSAT	−0.64	4.14	0.52	3.92	−0.15	5.20	1.78	3.06	0.78	2.33	0.51	2.15
GEOS-Chem in situ	−1.89	4.09	0.39	3.85	0.46	4.56	−0.26	2.69	−0.57	2.28	0.12	2.01
GEM GOSAT	−0.91	3.97	0.73	3.78	−2.64	5.16	0.40	2.77	0.27	1.24	1.03	1.44
GEM in situ	−2.01	3.96	0.26	3.76	−1.58	4.91	−1.25	2.77	−0.97	1.18	0.59	1.63
No. obs.	2137		1961		1388		2032		2125		2184	
South Pole												
	DJF 2010		MAM 2010		JJA 2010		SON 2010		DJF 2011		MAM 2011	
GEOS-Chem GOSAT	0.22	0.18	0.52	0.16	0.29	0.11	0.52	0.12	0.49	0.20	0.56	0.17
GEOS-Chem in situ	0.19	0.17	0.05	0.15	−0.22	0.10	0.15	0.18	0.21	0.24	0.03	0.15
GEM GOSAT	0.67	0.22	1.23	0.17	1.27	0.09	1.23	0.15	1.09	0.21	1.29	0.13
GEM in situ	0.68	0.18	0.69	0.13	0.66	0.10	0.76	0.10	0.76	0.20	0.66	0.13
No. obs.	2027		2111		2103		2055		2035		2120	

late CO_2 and search for instances of convolution of transport model errors. Figure 5 shows 2-year time series of modelled and measured CO_2 at the NOAA or ECCC stations of Alert, Mauna Loa, Sable Island and South Pole. Both model simulations use the flux estimates obtained with in situ observations. At Alert, which is far from CO_2 sources and sinks, a good comparison between the model simulation and measurements indicates a good ability of the model to transport the PAAF from the mid-latitudes to the high latitudes on seasonal timescales. Indeed, Fig. 5 shows that both model simulations agree rather well with observations at Alert with in situ posterior fluxes. In boreal summer GOSAT-retrieved fluxes produce a better match than in situ-based fluxes for both models (Table 2). The better match with observations in boreal summer is consistent with the increased density of GOSAT observations in the Northern Hemisphere at that time (Byrne et al., 2017). The overestimation in boreal spring of both years with GOSAT-based fluxes (Table 2) was also seen in Deng et al. (2016) and suggests fortuitously similar transport by the two models to this location. The overall agreement of both GEM-MACH-GHG simulations with Alert measurements is rather good, especially considering the poorer agreement obtained with CarbonTracker 2013B (Peters et al., 2007, http://carbontracker.noaa.gov, last access: 7 August 2018) fluxes in Polavarapu et al. (2016). This does not mean that GEOS-Chem posterior fluxes are superior in any way to those of CT2013B, but rather that the transport errors of GEOS-Chem and GEM-MACH-GHG are fortuitously commensurate, at this location and time period. At Mauna Loa and Sable Island, which are far from

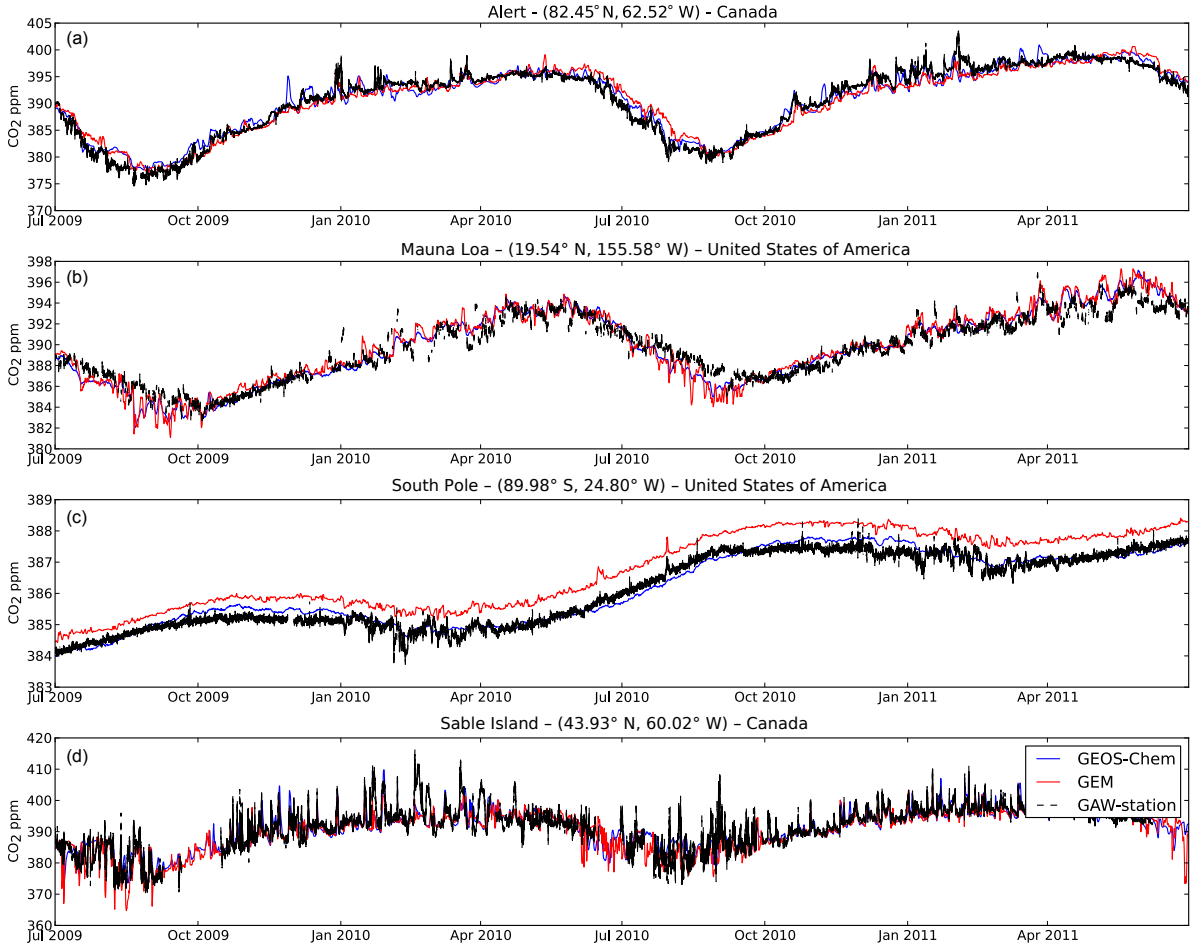

Figure 5. Time series of CO_2 observations and model simulations for 1 July 2009 to 1 July 2011. The CO_2 observations are from ECCC or NOAA GHG in situ measurement networks for Alert **(a)**, Mauna Loa **(b)**, South Pole **(c)** and Sable Island **(d)**. The observations are indicated in black. The model simulations with GEM-MACH-GHG (red curves) and GEOS-Chem (blue curves) used posterior fluxes obtained from inversions with GEOS-Chem using in situ observations.

sources but are also affected by synoptic-scale variability, both model simulations compare well to measurements. At the South Pole, any differences in transport errors between the two models that accumulate over long timescales are visible. Here a bias appears but it is mostly (~ 0.5 ppm) due to the regridded initial conditions with another 0.1 ppm arising after 2 years of simulation. The bias with GEM-MACH-GHG occurs with both sets of fluxes but the bias is smaller with in situ-based posterior fluxes (see also Table 2). From the bias in the simulation with in situ fluxes we infer a mismatch of transport times to the Southern Hemisphere between the two models since GEOS-Chem simulations with the in situ-based fluxes match this station's time series well (Table 2) and since a similar bias is also present between the two model simulations at other Southern Hemisphere stations (not shown). In addition, a positive bias of 0.5 ppm appears when GOSAT-based posteriors are used with GEOS-Chem (Table 2). Thus, the increased bias with GOSAT data is seen by both models (Table 2) and is a separate issue from the convolution of transport errors.

The GEOS-Chem inversion was performed with a coarse $4° \times 5°$ resolution grid, whereas GEM-MACH-GHG uses a much higher 0.9° resolution. So, the fact that the forward model simulations agree well with observations on synoptic timescales supports the contention of Agustí-Panareda et al. (2014) that the large-scale gradients of CO_2 are captured in the retrieved fluxes due to an adequate density of observations, whereas the high-resolution model captures and adds the correct synoptic-scale variability. Overall, we conclude that GEM-MACH-GHG simulates CO_2 reasonably well with GEOS-Chem fluxes on a variety of timescales in the Northern Hemisphere, but there is mismatch of transport times to the Southern Hemisphere. The fact that there are differences in the posterior CO_2 distributions with the two models (and evidence of convolution of transport errors) will inform dis-

cussions of atmospheric adjustments (PAAF and PAAM) in Sect. 3.

Polavarapu et al. (2016) showed that the existence of uncertainty in meteorological fields limits the spatial scales that can be depicted in CO_2 fields. Although it is only one of the many sources of error impacting CO_2 model distributions, it will always be present and may be considered a minimum error level. To estimate this error (PAAM), the forward simulations of GEM-MACH-GHG were repeated with perturbed meteorological fields and the difference in CO_2 defines this inescapable error. To perturb the meteorological fields, Polavarapu et al. (2016) simply computed the difference between the meteorological analyses valid at the required time and those valid 6 h prior to the required time, and then removed the diurnal signal from this perturbation. Here we improve on the methodology by using actual realizations of analysis error from our operational ensemble Kalman filter (EnKF) system (Houtekamer et al., 2014), which is used to determine meteorological forecast uncertainty on the medium range. Because the ensemble members were not available in the archives of the Canadian Meteorological Centre for the period of study here, we use analysis error estimates from a different year. The Supplement describes how the perturbations were computed and demonstrates that the method used to estimate analysis errors is considerably better that used in Polavarapu et al. (2016) despite some unavoidable approximations. In this work, meteorological fields perturbed by EnKF-derived meteorological analysis errors will be used to define minimum error levels in the diagnostics of Sect. 3.2.4 and 3.2.5.

As noted earlier, the diagnostic proposed compares PAAF and PAAM. However, PAAF depends not only on model errors but also on the chosen prior flux. Thus, the diagnostic provides assimilation system-specific information. To illustrate this dependency, time series of PAAF and PAAM sampled at the Sable Island location are shown in Fig. 6. PAAF (blue curve) increases throughout the period because the prior flux based on BEPS uses an annually balanced biosphere. Thus, for this site, PAAF contains a trend as well as seasonal and synoptic-scale variations. However, PAAM has no obvious trend or seasonal variations although synoptic-scale variability does depend on the season. A different prior flux would produce a different PAAF, perhaps lacking the trend seen in Fig. 6. Thus, the monitoring of PAAF may be useful for understanding the characteristics of a given assimilation system. As model errors and prior flux errors improve, PAAF will get smaller and the limiting uncertainty will become the meteorological analysis errors. At that point, the need for coupled meteorological and CO_2 assimilation will be evident for that system. Figure 6 also reveals that a site-specific comparison of PAAF and PAAM may be useful but requires careful interpretation. For example, the variability of PAAF exceeds that of PAAM in the summer of 2009 but not in the summer of 2010. Thus, the application of this diagnostic at individual sites is the subject of ongoing investigation. In the present work, we confine our attention to larger scales using diagnostics such as zonal means and zonal variability.

3 Results

The two sets of posterior fluxes that will be used to study the atmospheric CO_2 adjustments are described in Sect. 3.1 before considering the vertical structure of the PAAF in Sect. 3.2. While some of the figures below include results from both models, others show those from a single model. In such cases, results from the GEOS-Chem model are shown, while corresponding figures obtained with GEM-MACH-GHG are relegated to the Supplement. This choice was made because GEOS-Chem was used in the flux inversions, so posterior CO_2 distributions with GEOS-Chem are obtained with consistent model errors while posterior distributions obtained with GEM-MACH-GHG will convolve the transport errors from the two models. However, despite this convolution of errors, consistent patterns emerge with both models, lending greater confidence in the robustness of results in the face of transport error.

3.1 Posterior flux estimates

The inversion results used here are similar to those presented in Deng et al. (2014, 2016). However, we briefly present those results again here because (1) the runs used here are not identical (e.g. observation sets) to those published, and (2) we will be comparing the CO_2 adjustments arising from these two sets of fluxes so it is worth directly comparing them here.

The global total flux estimates for 2010 obtained from the two observation networks studied here are 5.01 Pg C (in situ) and 4.95 Pg C (GOSAT). Here positive values indicate fluxes from the Earth's surface into the atmosphere. The actual annual growth rate for 2010 from Conway and Tans (2012) is 2.41 ± 0.06 ppm or 5.12 ± 0.13 Pg C (using a conversion factor of 2.124 Pg C ppm^{-1}). The general agreement of both sets of posterior fluxes with the 2010 annual total flux suggests that both inversions are sufficiently well configured.

While the global annual totals for 2010 are similar with the two different observation networks, the spatial distributions of the fluxes for the 11 TransCom (Gurney et al., 2003) land regions differ (Fig. S6 in the Supplement). The prior and the in situ-based posterior fluxes are similar to those shown in Fig. 4 of Deng et al. (2014) while the GOSAT-based posterior fluxes are similar to those presented in Fig. 8 of Deng et al. (2016). As in Deng et al. (2014), Fig. S6 reveals that in situ data result in more uptake in the Americas, whereas fluxes retrieved from GOSAT data put more uptake in Eurasia. As noted in the Introduction, this increase in European uptake with GOSAT data was also seen by Reuter et al. (2014) and Houweling et al. (2015). In the north–south direction, in situ fluxes produce more uptake in the three tropical regions com-

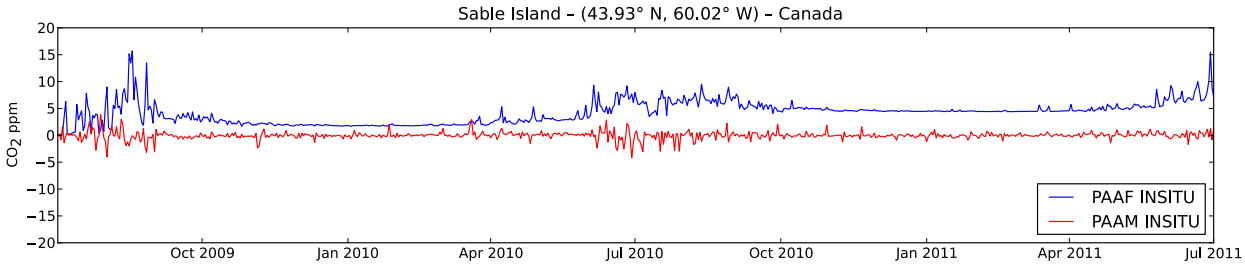

Figure 6. Time series of PAAF (blue curves) and PAAM (red curves) using in situ-based posteriors sampled at Sable Island for 1 July 2009 to 1 July 2011.

pared to GOSAT-derived fluxes, while the latter have relatively more uptake in temperate and boreal Eurasia. This was also seen in Houweling et al. (2015). This difference in north–south distributions of fluxes is more readily evident in Fig. 7, which shows the temporal variation of the fluxes accumulated over three large latitudinal bands: the northern extratropics, the tropics and the southern extratropics. (Here the dividing latitude between the tropics and extratropics is taken to be 19.47° or $\sin^{-1}(1/3)$ because it results in exactly equal areas for all three regions. This advantage is exploited later to interpret the diagnostics of Sect. 3.2.) Figure 7a reveals that both sets of fluxes are generally similar on the global scale, with two exceptions: (1) the peak boreal summer uptake occurs in June with GOSAT data, but in July with in situ data, and (2) GOSAT data produces larger outgassing of CO_2 in October and November. The larger outgassing with GOSAT data in boreal autumn is due to larger contributions from both the northern extratopics (Fig. 7b) and the tropics (Fig. 7c). The larger global uptake in June with GOSAT data is due to the northern extratropics (Fig. 7b). In the southern extratropics, GOSAT generally results in more uptake than in situ data, but the magnitude of the uptake and the difference between the two posterior fluxes is small (Fig. 7d).

In summary, the posterior fluxes produced here bear similarities to those produced by other inversion systems constrained by similar observation sets and are consistent with the range of results of the multi-inversion intercomparison of Houweling et al. (2015). Thus, the two sets of posterior fluxes may be considered to be reasonable examples representative of the two observing systems. Furthermore, the results obtained here should be relevant to other flux inversion systems.

3.2 Vertical propagation of the PAAF

Given the two sets of posterior fluxes, we now consider how they inform atmospheric CO_2 distributions. Although column measurements contain information about CO_2 concentrations throughout the depth of the troposphere, ultimately, in a flux inversion, this information is used to update a surface flux. It is unclear how this updated surface flux perturbation is then vertically transported to inform the middle and upper troposphere. Intuitively, one might expect the assimilation of column measurements to result in better CO_2 depictions in the middle and upper troposphere. However, as will be shown, this is not necessarily the case.

3.2.1 Zonal mean patterns

The PAAF was computed for both sets of posterior fluxes, resulting in four sets of 4-dimensional CO_2 fields – two sets for each model. To encapsulate the vertical motion, zonal mean fields were computed. The GEOS-Chem fields are animated in Fig. S7 and snapshots from the animation, taken every 3 months from 1 October 2009 to 1 July 2011 are shown in Fig. 8. Qualitatively similar results are obtained with GEM-MACH-GHG (Fig. S9). Immediately obvious from Fig. 8 is that the PAAF is largely negative for both experiments at all times. This occurs because the prior flux has a terrestrial component that produces an annually balanced biospheric flux. Thus, the fact that the terrestrial biosphere annually takes up approximately 30 % of the anthropogenic emissions entering the atmosphere (Le Quéré et al., 2015) is not assumed by the prior fluxes. This is done intentionally because of the desire that observations determine the existence and amount of uptake by the terrestrial biosphere. Here, the impact of using annually balanced biospheric fluxes and ocean prior fluxes from Takahashi (2009) that only account for 1.4 of the expected 2.5 Pg C yr^{-1} uptake is that the prior CO_2 distribution has a continually increasing global total relative to the actual increase. Then, once the flux inversion is performed and the fluxes are pulled toward realistic values, the posterior distributions reduce the overestimated CO_2. Thus, the difference between the posterior and the prior CO_2 distributions is always negative, in a global sense – hence the overwhelming negative values seen in Fig. 8.

Comparing the distributions obtained with the two observing systems reveals some clear patterns. In October 2009 (which is still in the spin-up period), the patterns are similar except that the GOSAT data produce a smaller PAAF in the tropics. This is even more evident by January 2010, where the GOSAT-derived PAAF has smaller CO_2 adjustments in the Northern Hemisphere as well. At this time, there is a clear difference in the vertical gradient of the PAAF between

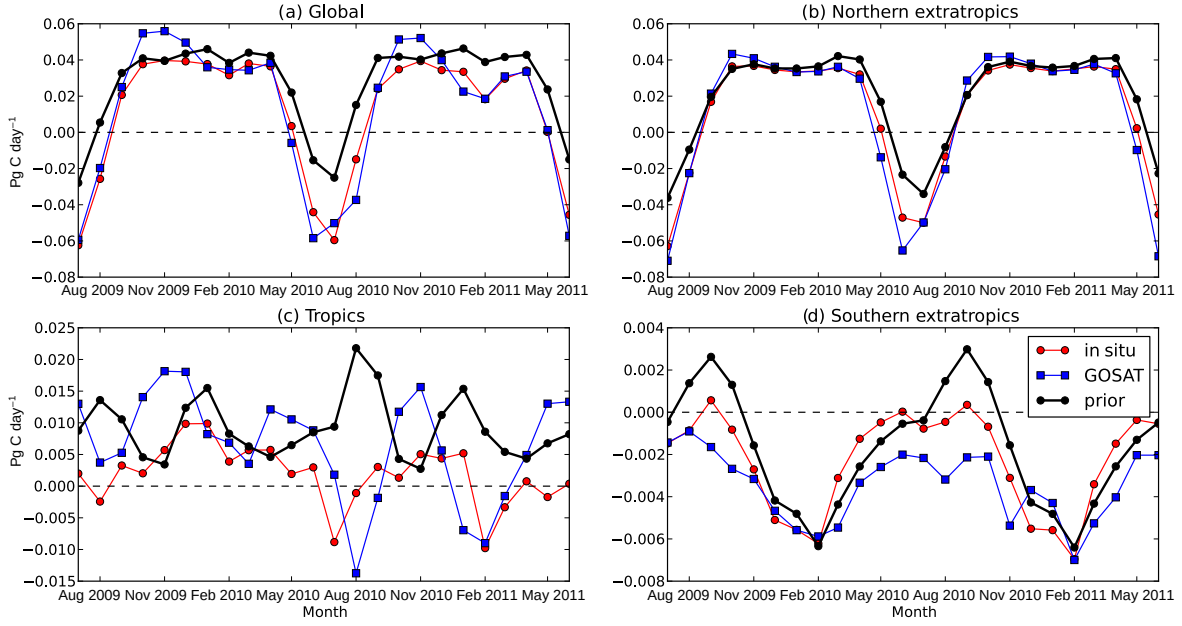

Figure 7. Prior and posterior fluxes area weighted and regionally averaged over **(a)** the whole globe, **(b)** the northern extratropics, **(c)** the tropics and **(d)** the southern extratropics. Fluxes are monthly averages from July 2009 to June 2011. Note the expanded vertical scales for panels **(c)** and **(d)**.

the tropics and northern extratropics, and GOSAT data produces reduced meridional gradients. This was also seen by the inversion systems in Houweling et al. (2015, their Fig. 8), but the reduced gradient was not supported by independent measurements. By April 2010, the in situ data are continuing to reduce CO_2 in the Northern Hemisphere and tropics, while the GOSAT data seem to not have much impact. However, in July 2010, GOSAT data produce a large negative PAAF in the Northern Hemisphere when the satellite observes this region well (Fig. 2). However, the tropical upper troposphere retains a stronger PAAF with the in situ data. In the second year of simulation, these patterns are repeated as the troposphere slowly adjusts to more realistic global mean values resulting from the observationally constrained terrestrial biospheric uptake. Specifically, October 2010 sees similar patterns for the two simulations in the Northern Hemisphere and tropics while January 2011 reveals larger CO_2 (smaller adjustments) throughout the troposphere in GOSAT-based simulations. April 2011 again sees a greater reduction in CO_2 throughout the tropics with in situ data, so that the GOSAT-based PAAF is less negative throughout the troposphere. Finally, by the end of June 2011, the large PAAF obtained with GOSAT data is seen once again in the Northern Hemisphere while in situ data retain a large PAAF in the tropical troposphere. When these patterns are animated (Fig. S7), it appears that the in situ data provide a constant injection of information from northern hemispheric fluxes, which is transported upward and equatorward to inform the tropical middle and upper troposphere. GOSAT data provide large updates to fluxes in boreal summer in the Northern Hemisphere, but when boreal autumn comes and the satellite tracks shift southward, the PAAF diminishes. In boreal winter, GOSAT observes the Southern Hemisphere well, but the Northern Hemisphere dominates the global CO_2 seasonal variation (Keeling, 1960) and so GOSAT misses the Northern Hemisphere emissions and the PAAF diminishes in this hemisphere with subsequent missing transport of the PAAF to the tropics. In fact, Houweling et al. (2015) argue that this seasonal variation of GOSAT data coverage plays a role in amplifying the European sink. This difference in the seasonality between inversions with in situ and GOSAT data is also consistent with the results of Byrne et al. (2017). Although both simulations only adjust surface fluxes, the in situ-based posterior fluxes constantly inform the Northern Hemisphere and the adjusted CO_2 patterns are transported upward to the tropics. This transport of information relies on the accuracy of the model's transport and hence may not be correct. Transport error has long been known to be a major source of error in flux inversion systems (e.g. Chevallier et al., 2014, 2010; Houweling et al., 2010; Law et al., 1996). Thus, to see which of the two posterior fluxes better depicts the middle and upper troposphere, we compare it to independent measurements in the next subsection.

3.2.2 Comparison to observations

Since the PAAF is defined as the CO_2 change relative to a given prior, it is not clear which pattern is more correct when the PAAFs are compared. Thus, in order to inform subse-

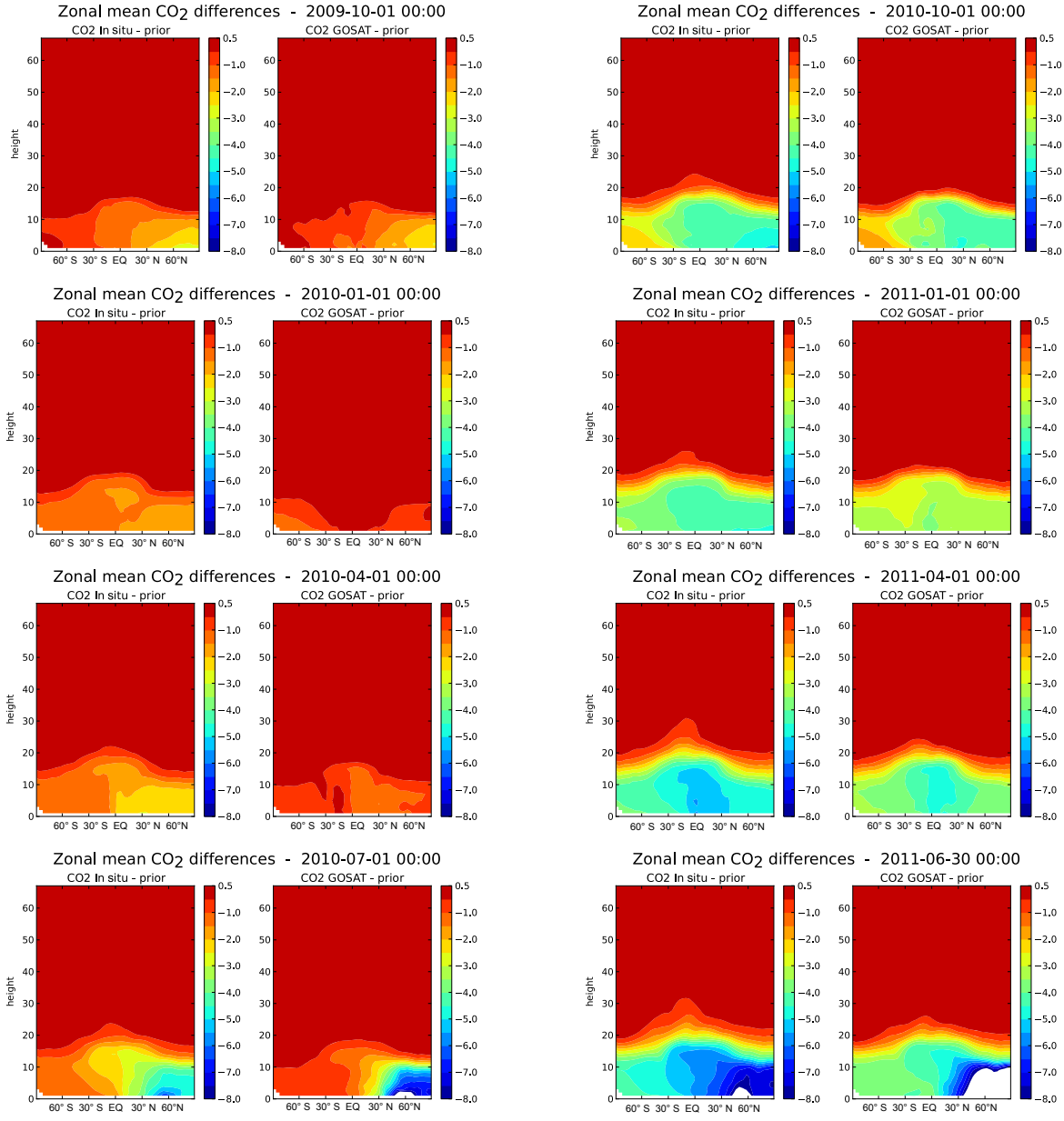

Figure 8. Time sequence of zonal mean posterior atmospheric adjustment due to fluxes (PAAF) simulated with GEOS-Chem. Zonal mean fields are displayed as a function of height and latitude in units of parts per million (ppm). Shown are the in situ (leftmost of each pair) and the GOSAT (rightmost of each pair) zonal mean PAAFs. The earliest date is in the top left corner with subsequent dates following down the left side then continuing down the right side. Dates are indicated above each pair of panels starting on 1 October 2009 and continuing in 3-month intervals to 30 June 2011.

quent discussions about PAAF diagnostics, we compare CO_2 posteriors directly to independent measurements. Total column measurements from the TCCON provide indirect information about CO_2 concentrations throughout the troposphere. The dominant feature seen in seasonally aggregated comparisons of modelled CO_2 to TCCON is the larger bias resulting from GOSAT-based fluxes (Figs. 9, 10). At all stations, except Eureka, a difference of about 0.5 ppm between the biases of the two simulations is present, with in situ data providing a closer fit to the measurements (Fig. 9). However, if we look beyond this time-mean bias (by subtracting it out), GOSAT-based fluxes are seen to better define the seasonal cycle (Table S1 in the Supplement) at most northern extratropical sites. Visually, this means the black curves are generally flatter than the red curves in Fig. 10. At most of the northern sites (Białystok, Garmisch, Izaña, Karslruhe, Lam-

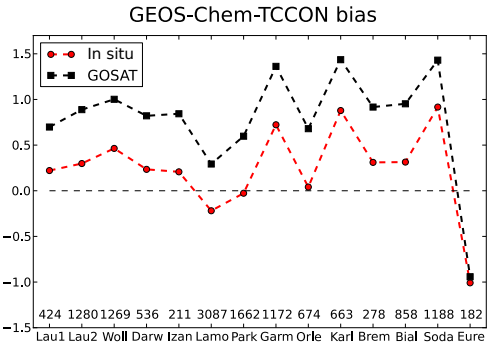

Figure 9. Comparison of GEOS-Chem CO_2 simulations with GOSAT-derived (black) and in situ-derived (red) posterior fluxes to TCCON measurements at 14 sites (Darwin, Wollongong, 2 instruments at Lauder, Izaña, Lamont, Park Falls, Garmisch, Orléans, Karlsruhe, Bremen, Białystok, Sodankylä, and Eureka). Stations are ordered by latitude from southernmost to northernmost. The mean residual in parts per million (ppm) was computed for each stations from December 2009 to May 2011, inclusive. Positive values mean the modelled CO_2 is generally higher than observed CO_2.

ont, Orléans, Park Falls, Sodankylä) the seasonal variation of the statistics obtained with GOSAT is better since the means of absolute anomalies are lower than those obtained with in situ data (compare columns 6 and 7 in Table S1). (The results from Eureka seem anomalous relative to other TCCON sites so this is a topic currently under investigation by Kimberly Strong (Dept. of Physics, University of Toronto, personal communication, 2017). Explanations under consideration include sampling issues, site-to-site differences, model transport errors and unknown issues with the data.) The improved ability of inversions constrained by GOSAT data to capture the seasonal cycle was also found by previous analyses (e.g. Deng et al., 2014; Liu et al., 2014; and Reuter et al., 2014). Butz et al. (2011) and Lindqvist et al. (2015) showed that ACOS GOSAT data alone can match the seasonal cycle at TCCON locations (typically within 1 ppm in the Lindqvist et al. study). In addition to better capturing the seasonal cycle, the GOSAT-based simulations result in lower mean residuals at many of the Northern Hemisphere sites in June, July and August (Fig. 10). Improved agreement with independent observations using posterior fluxes from the GOSAT inversion relative to the in situ inversion during boreal summer was also found by Basu et al. (2013), Deng et al. (2014) and Reuter et al. (2014) and suggests that the summer drawdown in the in situ inversions is too weak over the northern extratropics. Overall, however, the posterior fluxes obtained with in situ observations provide better agreement with TCCON overall since 61 of the 76 (80 %) comparisons favour the simulation based on in situ data (Fig. 10). The standard deviations are rather similar for the two simulations and are frequently smaller than the means (Fig. 10).

Comparisons to TCCON obtained with GEM-MACH-GHG posterior CO_2 distributions are found in Figs. S10 and S11. The same conclusions hold: there is an overall larger mean mismatch with TCCON when GOSAT-based posteriors are used (Fig. S10) but the seasonal cycle is better captured at most northern extratropical sites (Table S1) and the agreement in boreal summer is better at many northern extratropical sites (Fig. S11). Additionally, a larger bias with TCCON at Southern Hemisphere sites is seen with GEM-MACH-GHG compared to that obtained with GEOS-Chem (Fig. 9). This bias was also seen in Fig. 5 (South Pole station) and arises mainly from the initial condition but is affected by the differing transport times from the tropics to the Southern Hemisphere in the two models. GEOS-Chem transports CO_2 more rapidly to the Southern Hemisphere and its posterior fluxes reflect this rapid transport (see animation in Fig. S8, especially July–August 2010). When inserted into GEM-MACH-GHG, the fluxes obtained assuming a fast transport to the Southern Hemisphere result in a too-slow departure from the prior CO_2 distribution and a larger bias with respect to observations. However, because GEM-MACH-GHG is disadvantaged by the convolution of transport errors, these results do not identify which model's interhemispheric transport to the south is more realistic. As a weather and environmental forecast model, knowledge of the age-of-air for GEM-MACH is not essential for its timescales of interest, so this work identifies a need to better characterize inter-hemispheric transport with the GHG version of this model. At the same time, this work shows little evidence for the convolution of transport errors on shorter timescales or in the Northern Hemisphere (as was seen when GEM-MACH-GHG used CT2013b fluxes in Polavarapu et al., 2016). Moreover, despite the existence of some convolution of transport errors, conclusions regarding the agreement with independent measurements hold for both models, increasing confidence in the robustness of results in the face of model errors.

A more direct assessment of middle and upper tropospheric CO_2 distributions is obtained by comparing to aircraft profiles. Comparisons of both GEOS-Chem simulations to measurements from the HIPPO-3 campaign in 24 March to 16 April 2010 are shown in Fig. 11. The results are aggregated by latitude and vertical bands. The in situ-based posterior fluxes result in lower mean differences from measurements in the middle to upper troposphere (panel c) and the lower stratosphere (panel d) in the northern extratropics. However, the GOSAT-based posterior fluxes generally agree better with measurements in the southern extratropics at all heights. Similar results are also obtained with GEM-MACH-GHG (Fig. S12) in the northern extratropics, but in the southern extratropics, in situ fluxes better match observations because of initial condition differences and the convolution of transport errors, which leads to increased CO_2 in the Southern Hemisphere for all fluxes. Note that in the stratosphere for both comparisons with HIPPO-3 (Figs. 11d and S12d), the mean mismatch exceeds the standard deviation. This means that both model simulations are biased in the stratosphere, as was seen in Deng et al. (2015). Such

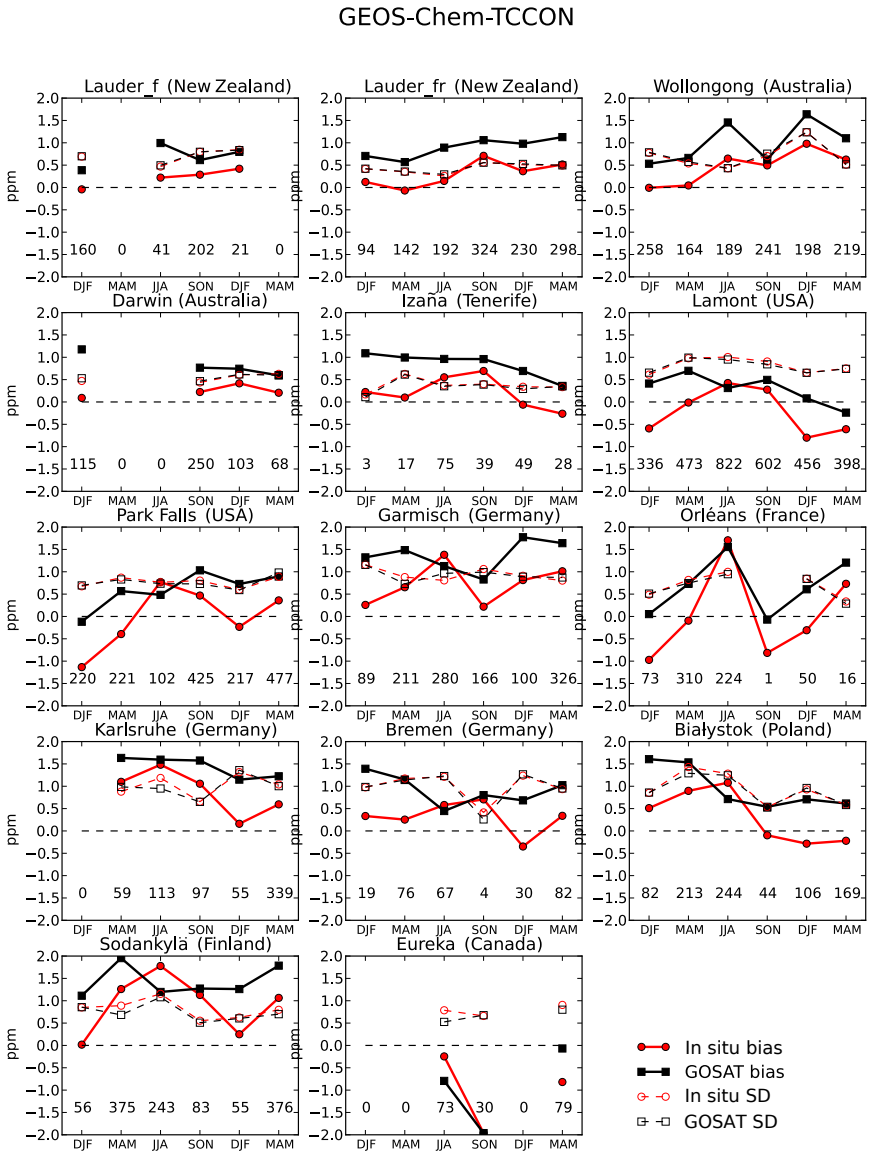

Figure 10. Comparison between TCCON measurements at 14 sites and the GEOS-Chem CO_2 simulations driven with posterior fluxes from the GOSAT (black) and in situ (red) inversions. Scores (bias and standard deviation) are aggregated by 3-month seasons from December 2009 to May 2011. Lauder appears twice because there are two different instruments there.

a bias can adversely affect flux estimates in the Northern Hemisphere (Deng et al., 2015). Comparing Figs. 11 and S12 (panels c and d) reveals that GEM-MACH-GHG has better agreement with HIPPO-3 than does GEOS-Chem in the middle to upper troposphere and in the stratosphere. This makes sense given the finer vertical and horizontal resolution of GEM-MACH-GHG and is expected from the results of Deng et al. (2015, their Figs. 11–12). The number of realizations used in each comparison in Figs. 11 and S12 ranges from 94 to 2570 and the differences in the mean values of the two experiments are significant at the 90 % level. Thus, overall, we conclude that the middle and upper tropospheric distributions of CO_2 are better in the Northern Hemisphere in boreal spring 2010 when posterior fluxes use in situ data rather than GOSAT column measurements.

Since measurement campaigns occur only in select time windows (HIPPO-3 was in March–April 2010), we also consider the more routine NOAA aircraft profile measurements from continental US and Canadian sites in Fig. 12. The observations are from ObsPack2013 (Masarie et al., 2014). As in Agustí-Panareda et al. (2014), mean model profiles at the nearest grid point and time step to the observation locations and times are averaged over a season. Observed values are binned into 1 km layers and compared to model values at mid-layer. Hourly GEOS-Chem fields are used. When the entire 2010 year is considered, the bias throughout the tro-

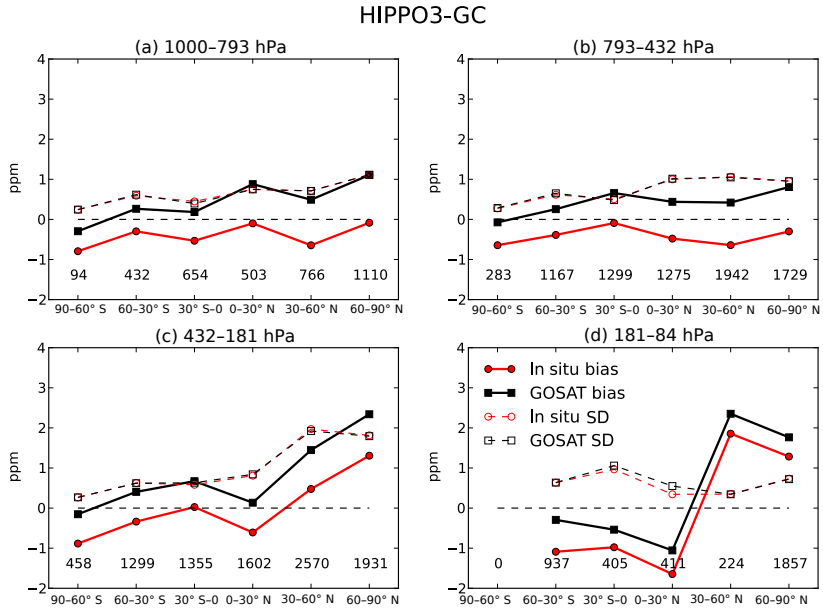

Figure 11. Comparison between the HIPPO-3 measurements and the GEOS-Chem CO_2 simulations driven with posterior fluxes from the GOSAT (black) and in situ (red) inversions. Scores (bias and standard deviation) of modelled minus observed values are aggregated by latitude band and over the pressure layers given above each panel. The numbers of observations used in each statistic are indicated within each panel. The flights occurred between 24 March to 16 April 2010.

posphere with respect to the aircraft profiles is much smaller with in situ-based posterior fluxes (Fig. S13) for both models. However, the results are more variable if broken down by season. In boreal winter, in situ data produce better agreement with NOAA aircraft near the surface but from 2 to 6 km GOSAT data give a better result (Fig. 12). This variation in fit is related to the fact that vertical profiles from GEOS-Chem have stronger than observed gradients in the lowest 1–2 km. GEM-MACH-GHG profiles better match observed gradients (Fig. S14) and GEM-MACH-GHG profiles consistently favour the same simulation in both height ranges. In December–February 2010, the in situ-based simulation better matches observations although it is partly in the spin-up period, whereas in December–February 2011, the GOSAT-based simulation better matches mean NOAA aircraft profiles at all heights (Fig. S14). In boreal spring (Figs. 12 and S14) in situ data produce better agreement not just near the surface, but at all heights. In boreal summer, GOSAT data result in much better agreement from 1 to 3 km but from 3 to 6 km there is little difference between the two simulations. However, in boreal autumn, GOSAT data achieves a better match from 2 to 6 km, whereas in situ data has a better match near the surface (Fig. 12). As in boreal spring, incorrect vertical gradients obtained with GEOS-Chem are likely playing a role in the inconsistent results since GEM-MACH-GHG's vertical gradient is closer to that observed and it favours the GOSAT-based simulations at all heights (Fig. S14). Overall, from 3 to 6 km, simulations with both posteriors produce similar model profiles in boreal summer and fall, but in boreal winter and spring there is a difference between the two, with in situ data producing lower CO_2. The lower CO_2 values obtained with in situ data agree better with aircraft data in boreal spring, but not in boreal winter. From 1 to 2 km, in situ data better match aircraft data in boreal spring while GOSAT achieves the better match in boreal summer, for both models. These results once again confirm that in boreal summer when GOSAT views and samples the Northern Hemisphere well, the estimated fluxes are improved in the lower troposphere.

In summary, the results that are consistent are as follows. (1) Despite the reliance on faithful model transport, in situ-based posterior fluxes produce CO_2 distributions that better agree with independent observations of the middle troposphere in the Northern Hemisphere in boreal spring. This may partly be due to the propagation of the near-surface improvements obtained in boreal winter. (2) GOSAT-based posterior fluxes consistently achieve better agreement with independent observations in the Northern Hemisphere in boreal summer and in the middle to upper troposphere in boreal winter.

3.2.3 Adjoint sensitivity

Figures 8 and S9 as well as animated Figs. S7 and S8 imply a propagation of the PAAF from the northern mid-latitude lower troposphere to the tropical middle and upper troposphere with in situ-based posterior fluxes. The question of whether this is realistic or not was the subject of the previous

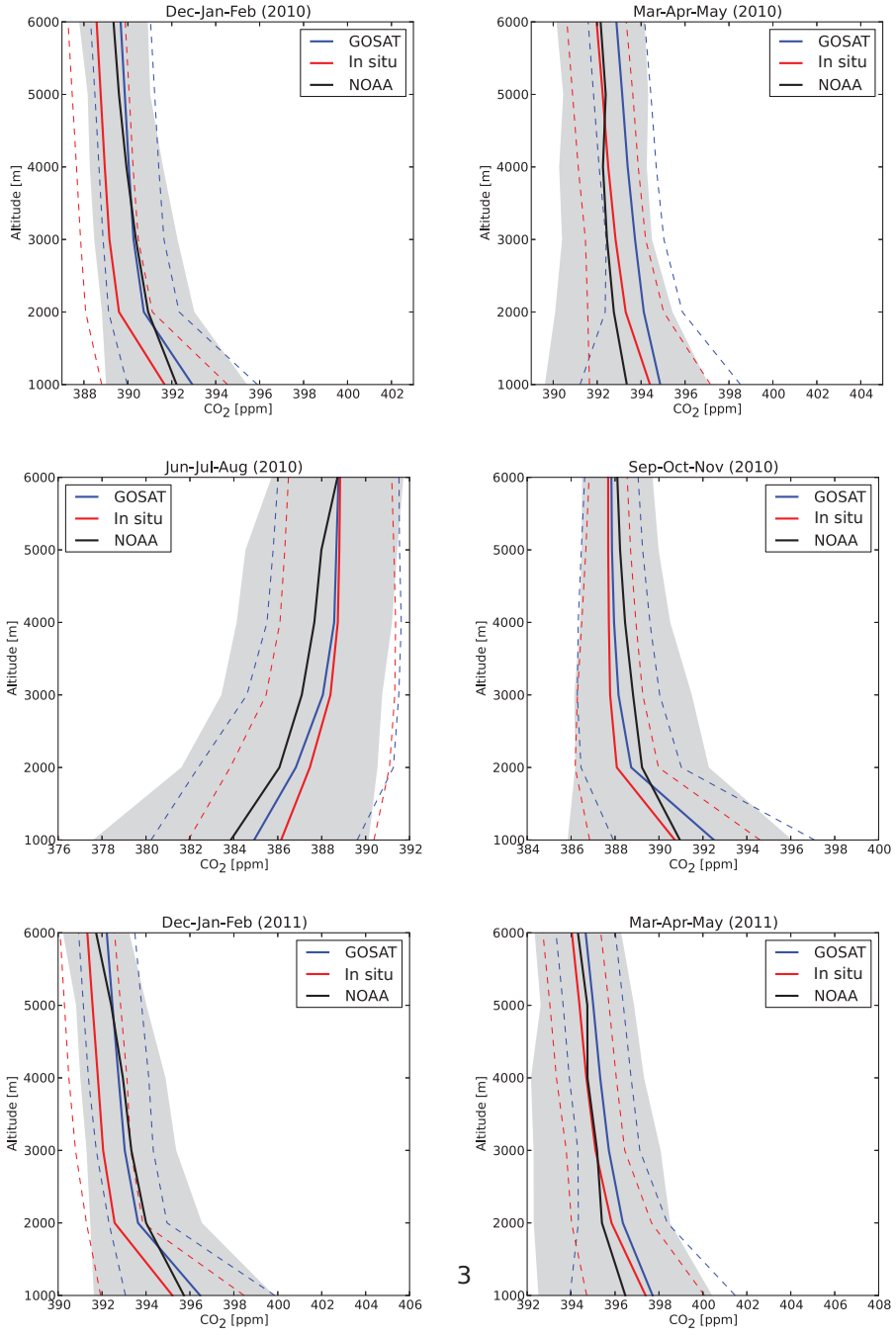

Figure 12. Comparison of mean GEOS-Chem model profiles of CO_2 to NOAA aircraft observations. Observations (black curves) are from obspack_co2_1_PROTOTYPE_v1.0.4_2013-11-25 for locations over continental US and Canada, only. Observed and modelled profiles are binned over 3-month seasons as indicated above each panel. Model simulations used posterior fluxes from GEOS-Chem inversions with GOSAT (blue) or in situ (red) observations. The shaded grey regions indicate plus or minus one standard deviation for the observations while the dashed coloured lines indicate the same quantities but for the different model runs. Sites used are Beaver Crossing, Nebraska; Bradgate, Iowa; Briggsdale, Colorado; Cape May, New Jersey; Charleston, South Carolina; Dahlen, North Dakota; East Trout Lake, Saskatchewan; Estevan Point, British Columbia; Fairchild, Wisconsin; Harvard Forest, Massachusetts; Homer, Illinois; Oglesby, Illinois; Park Falls, Wisconsin; Poker Flat, Alaska; Sinton, Texas; Southern Great Plains, Oklahoma; Trinidad Head, California; West Branch, Iowa; Worcester, Massachusetts.

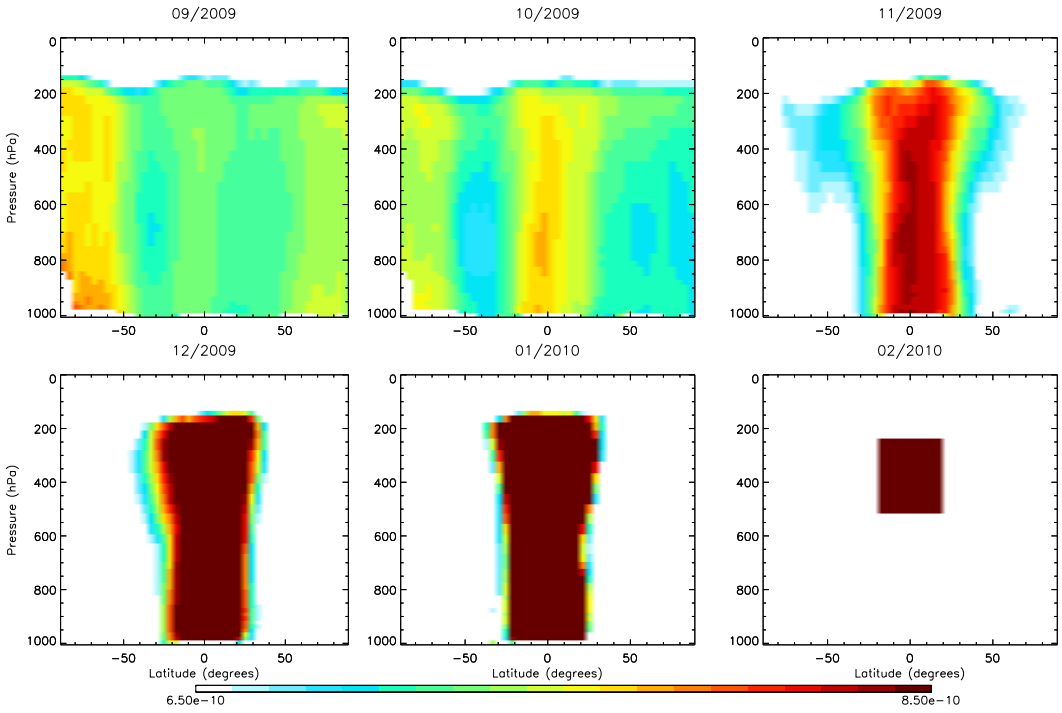

Figure 13. Sensitivity (in ppm ppm^{-1}) of the GEOS-Chem tropical tropospheric CO_2 on 1 February 2010 to the 3-D modelled state on earlier dates. Sensitivity fields are zonally averaged instantaneous fields for the first day of each month from September 2009 to February 2010 in the various panels.

subsection where model simulations were compared to independent observations. Here we consider whether such transport (realistic or otherwise) has implications for flux inversions. In other words, can CO_2 from the northern extratropics influence the CO_2 in the tropical upper troposphere a few months later? To see whether this occurs in the flux inversion system, we compute the sensitivity of CO_2 at one point in time with respect to the CO_2 state at an earlier point in time using the adjoint of GEOS-Chem (Henze et al., 2007). While Byrne et al. (2017) utilize the adjoint sensitivity with respect to surface fluxes, here we need to consider the entire CO_2 state in order to see vertical transport of information. The extension of the adjoint calculation needed to produce sensitivity to the CO_2 state is described in Appendix A, and Fig. 13 shows the sensitivity of the CO_2 field on 1 February 2010 to earlier states, at 1 month intervals. Each panel shows a snapshot of the zonally averaged sensitivity field. In February 2010, the sensitivity is initialized to a uniform value within a mask from 20° S to 20° N and 500 to 250 hPa. Proceeding backward in time, this field is sensitive to the CO_2 field throughout the depth of the tropics in January 2010 with a hint of sensitivity beyond the tropics in the stratosphere. By November 2009, this stratospheric influence is more evident and by October 2009, extratropical tropospheric influence is also evident. By September 2009, the sensitivity is largest in the northern and southern extratropics. Tracing the pattern in the Northern Hemisphere forward in time through the panels reveals upward and equatorward propagation of the signal. Thus, the CO_2 field in the northern tropics in the upper troposphere in boreal spring is sensitive to CO_2 in the northern mid-latitude lower troposphere on 1 September. In other words, observations near the surface at northern mid-latitudes on 1 September can potentially impact CO_2 fields in the tropical upper troposphere, 3 to 6 months later. Because the adjoint calculation only reveals patterns without a magnitude (since the actual influence of an observation on CO_2 estimates also involves error covariances of observations and propagated prior flux errors), only a potential influence can be revealed in Fig. 13. However, this potential influence is sufficient to demonstrate the atmospheric transport from the northern mid-latitude lower troposphere to the tropical upper troposphere on the timescale of several months. This figure then supports the notion that observations of the northern mid-latitudes combined with model transport can influence (rightly or wrongly) CO_2 distributions downstream in the middle and upper tropical troposphere.

3.2.4 Global mean posterior atmospheric adjustments

Flux perturbations modify CO_2 fields locally but, eventually, gradients get diffused by atmospheric turbulence and only the impact on the background CO_2 field is retained. Thus, looking at the zonal or global mean PAAF reveals long-timescale information retained from flux adjustments after

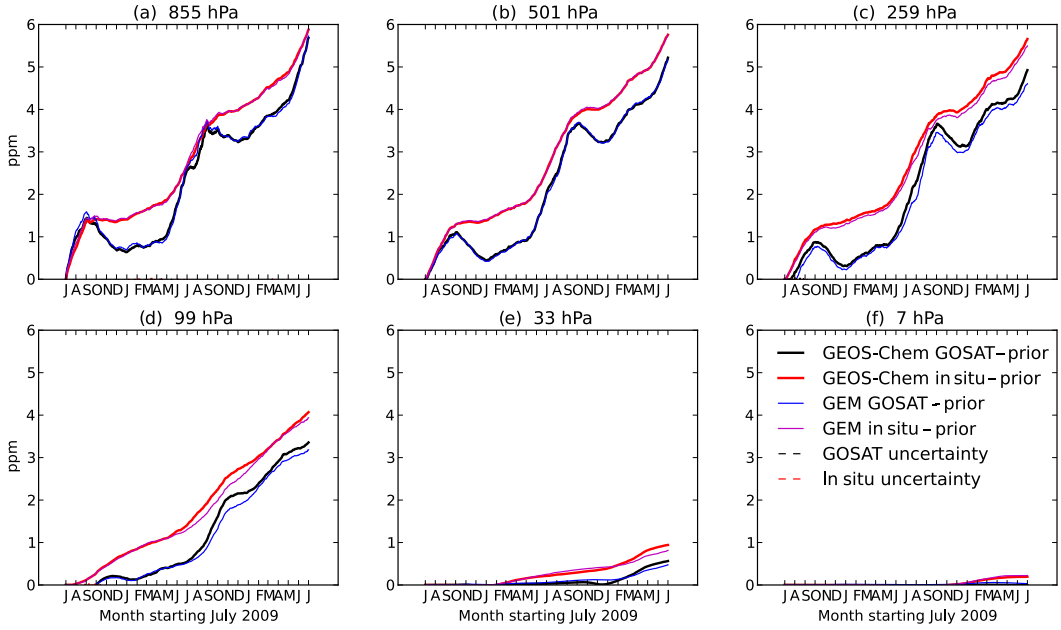

Figure 14. Global mean CO_2 PAAF for 1 July 2009 to 30 June 2011 from the GOSAT-based posterior fluxes (solid black curves) and the in situ-based posterior fluxes (solid red curves). PAAFs (prior minus posterior CO_2 fields) are shown for the model level closest to the nominal pressure level, indicated above each panel for both GEOS-Chem (thick lines) and GEM-MACH-GHG (thin lines). The global means of the CO_2 uncertainty are shown for the GOSAT posterior flux integration (black dashed curves) and the in situ posterior flux integration (red dashed curves) but are not visible because they are negligible. Uncertainty in CO_2 is estimated with GEM-MACH-GHG by perturbing the meteorological analyses and computing the difference from the unperturbed integration.

redistribution and dispersion by model transport. How long does it take for a flux perturbation to modify the background CO_2 state? Deng et al. (2014) show that transit times of regional fluxes to the middle troposphere further downstream are shorter than 2 months and flux perturbations have dispersed to the background within 3 months (see their Fig. 15). Similarly, Liu et al. (2015) found that column measurements are unable to distinguish the locality of fluxes older than three months. Figure 14 shows the global mean PAAF for both models and both observing systems at selected model levels in the lower troposphere (panel a), the middle troposphere (panel b), the upper troposphere (panel c), the lower stratosphere (panel d), the middle stratosphere (panel e) and the upper stratosphere (panel f). (It was possible to find similar model levels in terms of approximate pressure for the six representative pressures for the two models by assuming a 1000 hPa reference for each vertical coordinate. These are listed in Table 1.) From Deng et al. (2014) and Liu et al. (2015) we conclude that the timescales reflected in Fig. 14 are seasonal and longer timescales. The evolution of global CO_2 when forced by the prior flux is missing a trend due to the assumption of a balanced biosphere so the prior CO_2 fields drift from a realistic global mean, increasingly overestimating it. Since the posterior CO_2 fields are constrained by observations to resemble the actual atmospheric budget evolution, our global PAAF increases with time as the trend error accumulates (Fig. 14 black curves). (Here the posterior fields are subtracted from the prior fields to give positive values, for convenience.) Figure 14 shows that the global PAAF increases not only for the atmosphere as a whole but also at all heights (except the upper stratosphere). In addition, for the GOSAT-based PAAF, there is a large seasonal variation on top of the linear trend which has largest amplitude near the surface.

Figure 14 also shows that despite the differing transport errors, the global PAAFs are very similar for the two models. The largest differences occur in the upper troposphere and lower stratosphere (UTLS) regions (panels c and d). As noted by Deng et al. (2015), the GEOS-Chem CO_2 simulation at a resolution of $4^\circ \times 5^\circ$ is biased in the UTLS. Stanevich et al. (2018) found a similar bias in the coarse-resolution CH_4 simulation in GEOS-Chem, which they attributed to excessive mixing across the tropopause at the $4^\circ \times 5^\circ$ resolution. Also, as noted earlier, GEM-MACH-GHG compares better to HIPPO3 in the upper troposphere and stratosphere of the northern extratropics with the same posterior fluxes as GEOS-Chem. Compared to the PAAF obtained with in situ data, the PAAF derived from GOSAT data diminishes in boreal winter and spring throughout the troposphere. Recall that in boreal spring, in situ data provided the better match of CO_2 distributions to NOAA aircraft in the lower troposphere (Figs. 12, S14). In the stratosphere, the overall signal

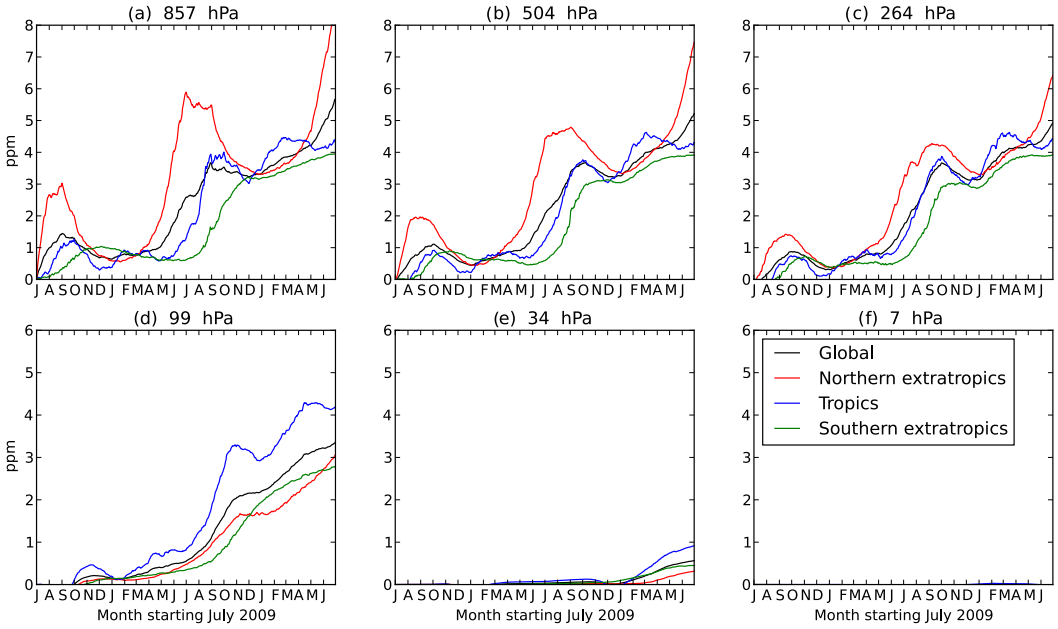

Figure 15. Global mean CO_2 PAAF obtained with GEOS-Chem with GOSAT-based posterior fluxes. PAAFs (prior minus posterior CO_2 fields) are shown for the model level closest to the nominal pressure level, indicated above each panel. The coloured curves represent the global total (black) and the contributions to this from the various subregions: northern extratropics (red), southern extratropics (green) and tropics (blue). Because the subregions were chosen to have equal areas, the contribution depicted for each subregion was scaled by a factor of 3 so that the mean of the contributions from the subregions gives the total contribution.

is smaller with GOSAT data, but there is little seasonality to the signal for either experiment (Fig. 14d–f). Because the PAAF reflects the departure of the posterior from the prior CO_2 field, it is not clear whether a large or small seasonal variation should be expected. However, comparisons of posterior fields to measurements in Sect. 3.2.2 revealed that the posterior CO_2 fields derived from in situ data have an approximately 0.5 ppm lower bias relative to TCCON at all sites except Eureka. They also agree better with NOAA aircraft and HIPPO-3 in the middle and upper troposphere in boreal spring and with NOAA aircraft at all heights when annual mean profiles are considered. This suggests that the larger signal seen in boreal spring with in situ data may be realistic. In boreal winter, near the surface, the CO_2 fields obtained from in situ posteriors agree better with NOAA aircraft profiles, but those based on the GOSAT posteriors yield better matches from 2 to 6 km. However, the NOAA aircraft data used corresponds to North America, whereas Fig. 14 illustrates global diagnostics while the overall TCCON comparison (Fig. 9) suggests in situ distributions are more realistic. Thus, it is not entirely clear whether the larger signal seen in boreal winter with in situ data is more realistic than the lower one obtained with GOSAT data. What is clear is that our flux inversions that assimilate GOSAT data produce posterior distributions that are less consistent with observations in global, annual statistics than flux inversions using in situ data. In addition, the GOSAT-informed PAAF has much stronger seasonal variations than the in situ-based PAAF. Thus, sub-annual variations in the global mean CO_2 adjustments are sensitive to the observing system used. However, this sensitivity also depends on the choice of prior fluxes since, for example, a prior flux with reduced bias in boreal summer would reduce this effect.

How much can we trust the global PAAF? The model transport of flux adjustments is not perfect and a major component of the transport model uncertainty is due to wind field errors (Liu et al., 2011). We can use the coupled meteorology and greenhouse gas transport model to identify the error due to wind field uncertainty on atmospheric adjustments by simply repeating each simulation with perturbed meteorological fields (as described in the Supplement) to compute PAAM. When PAAF and PAAM are comparable, PAAF is not the dominant component in our system and should not be accorded great significance. PAAM is plotted in Fig. 14 but is not evident because the curves are near zero. This is not surprising because the global mean atmospheric CO_2 is independent of transport. It is the spatial distribution of CO_2 that is affected by atmospheric transport (as will be demonstrated shortly). However, by considering the global mean at various heights, there was the possibility that an influence of errors in atmospheric transport might be seen at some vertical levels.

Figure 15 shows how the tropics and extratropics contribute to the global PAAF based on GOSAT data and computed with the GEOS-Chem model. As noted earlier, the di-

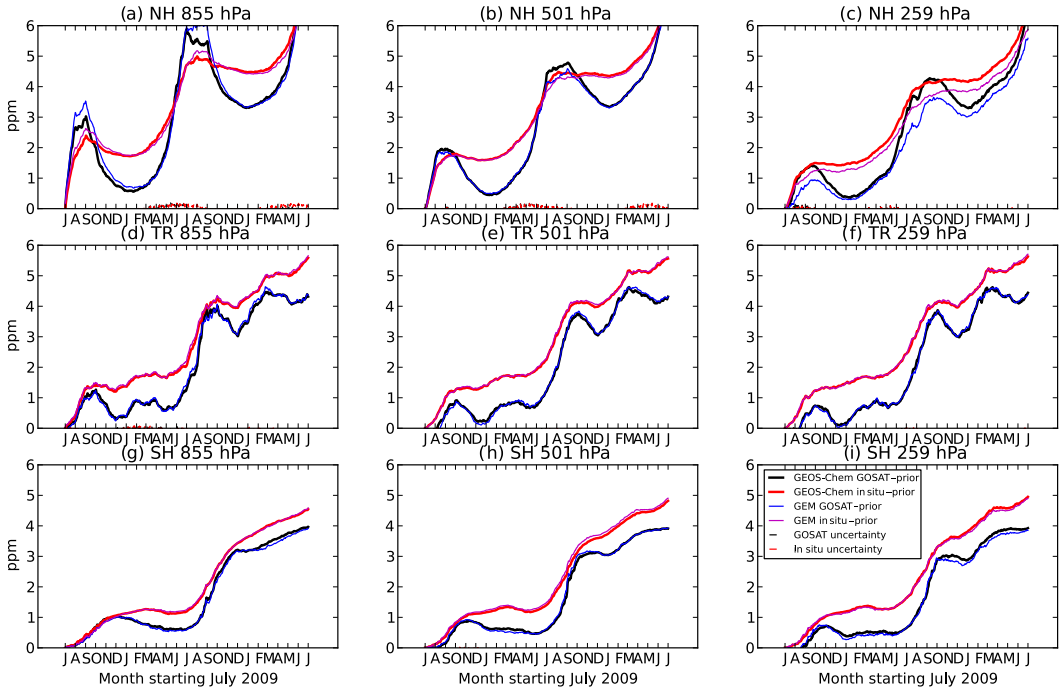

Figure 16. Regional contributions to the global mean CO_2 PAAF for 1 July 2009 to 30 June 2011. The PAAF is from the GOSAT-based posterior fluxes (solid black curves) and the in situ-based posterior fluxes (solid red curves). PAAFs (prior minus posterior CO_2 fields) are shown for the model level closest to the nominal pressure level, indicated above each panel for both GEOS-Chem (thick lines) and GEM-MACH-GHG (thin lines). Regional contributions have been multiplied by a factor of 3 as in Fig. 14. Uncertainty in global mean CO_2 is shown for the GOSAT posterior flux integration (black dashed curves) and the in situ posterior flux integration (red dashed curves). Uncertainty in CO_2 is estimated for each integration by perturbing the meteorological analyses and computing the difference from the unperturbed integration.

viding latitude between the tropics and extratropics was chosen so that the three zonal bands have equal areas. Because the zonal bands have equal areas, we multiply the zonal contributions depicted in Fig. 15 by a factor of 3, which means that each regional total (red, blue or green curves) can be compared to the global total (black curves). For example, Fig. 15a reveals that in the lower troposphere, the dominant contribution to the global PAAF comes from the northern extratropics where there is a large seasonal variation due to the seasonality of observational coverage (Fig. 2) in addition to the seasonality in the fluxes. This is also true for the middle troposphere (Fig. 15b). However, in the lower and middle stratosphere, the tropics dominate the global PAAF (Fig. 15d–e). The upper stratosphere is not much influenced by flux adjustments (Fig. 15f) on the 2-year time frame. Since the northern extratropics dominate the global PAAF, the concern of Houweling et al. (2015) that the excellent observational coverage of this region by GOSAT in boreal summer combined with the poorer coverage in boreal winter has implications on flux inversions seems warranted. Figure S15 shows that these patterns also occur for PAAFs derived from assimilating in situ observations but the seasonal variation of the PAAF is greatly reduced. The PAAF is largest in boreal summer due to adjustments in the northern extratropics for both posterior fluxes (Figs. 15 and S15). As seen in Fig. 8, these adjustments in July are much greater when GOSAT data is assimilated. Indeed Byrne et al. (2017) found GOSAT data are highly sensitive to boreal summer fluxes. This is also consistent with the large summertime flux adjustments of Liu et al. (2014) and the increased European fluxes seen from May to August in Houweling et al. (2015).

Figure 16 compares the regional contributions to the global PAAF for the two models. The differences seen in the UTLS in Fig. 14c are evidently due to differences seen in the northern extratropics (Fig. 16c) in boreal summer and autumn. Since GEM-MACH-GHG agrees better with HIPPO-3 in the middle and upper troposphere and in the lower stratosphere, it is possible that its signal is more accurate in this region. However, given the limited temporal and spatial domain of the measurements, such a conclusion would be tentative at best. The overall agreement between the two very different models suggests that the diagnostic is primarily seeing the impact of the posterior fluxes (which were the same for both models) for the large zonal bands considered. In addition, because the diagnostic involves a difference between model integrations, the Southern Hemisphere bias in CO_2 seen in GEM-MACH-GHG initial conditions is common to all simulations with this model and thus is subtracted out in

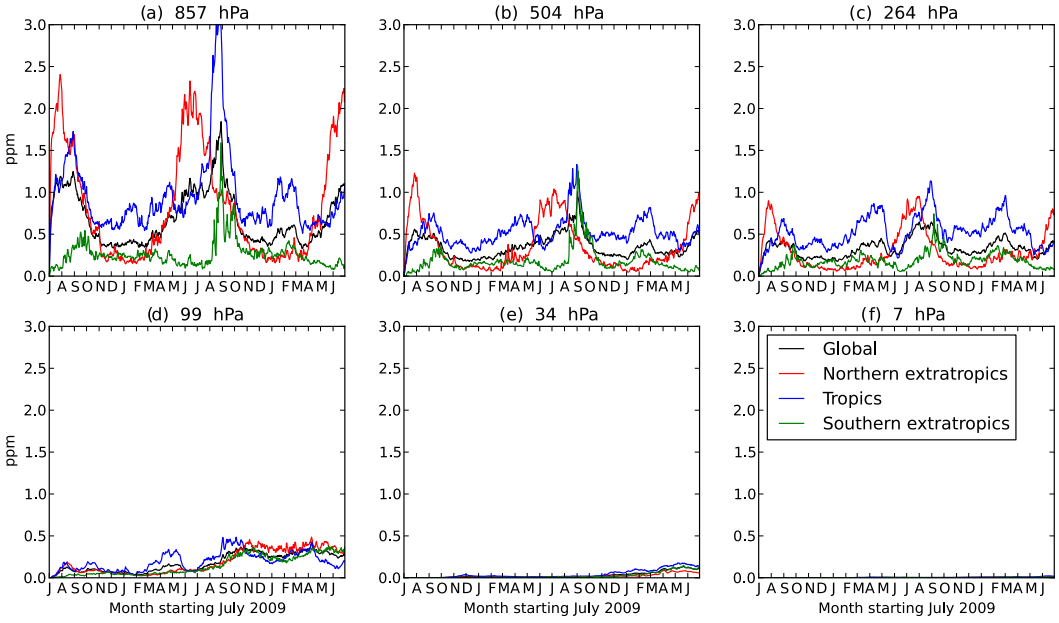

Figure 17. Contributions to global mean of zonal standard deviation of the CO_2 PAAF obtained with GEOS-Chem using GOSAT-based posterior fluxes. Statistics are shown for the model level closest to the nominal pressure level, indicated above each panel. The coloured curves represent the global total (black) and the contributions to this from the various subregions: northern extratropics (red), southern extratropics (green) and tropics (blue). Because the subregions were chosen to have equal areas, the contribution depicted for each subregion was scaled by a factor of 3 so that the mean of the contributions from the subregions gives the total contribution.

the PAAF and PAAM diagnostics. Figure 16 also shows that when the global mean is subdivided into three zonal bands, a tiny (negligible) influence of atmospheric transport errors associated with imperfect meteorology becomes apparent near the surface (Fig. 16a–b) in the northern extratropics during boreal spring and summer. In addition, the CO_2 adjustment due to wind field uncertainty (PAAM) exceeds the atmospheric adjustment obtained from assimilating either set of observations (PAAF) in the tropical upper stratosphere (not shown). Overall, however, the global PAAFs are very similar between the two models, even after dividing them into regional contributions.

3.2.5 Zonal asymmetry in the posterior atmospheric adjustments

Departures from zonal mean PAAFs can be used to examine shorter temporal and spatial scales in the PAAF. The zonal mean flow has no zonal standard deviation (by definition) so large zonal standard deviations indicate greater zonal structure (or asymmetry within a zonal band). Moreover, once the flux perturbation has diffused to the background (or zonal mean) state, it will not contribute to the zonal standard deviation. As noted earlier, in the troposphere, the flux perturbation diffuses to the background state in about 3 months. Thus, the zonal standard deviation field shown in Fig. 17 reflects shorter timescales than does the zonal mean of the PAAF. That explains why curves in Fig. 17 do not have a trend in the troposphere as was seen in Figs. 14–16. The zonal structure is largest in boreal summer in the lower troposphere (black curves in panels a–b) mainly due to the PAAF in the northern extratropics (red curves). The impact of large flux increments in boreal summer was also seen in zonal mean fields in Figs. 8 and S9. In addition, a rather constant and large zonal standard deviation is seen in the tropics (blue curve in Fig. 17a). This is consistent with the findings of Deng et al. (2016) and Byrne et al. (2017) that finer-scale flux estimates can be obtained in the tropics with GOSAT glint observations. However, in the middle troposphere and above, the seasonal variation in zonal standard deviation diminishes, as occurred with the zonal mean PAAF (Figs. 14–16). Also, the magnitude of the zonal standard deviation diminishes with height. In the stratosphere, while the magnitudes are small, a small trend is seen in the second year in panels (d) and (e). This suggests that after 1 year of simulation some zonal asymmetry is being seen in the PAAF and that transit times of surface flux perturbations to the stratosphere are longer than the 3 months needed to reach the mid-troposphere. This delayed response makes sense given that the mean age of air is about 1 year in the tropical lower stratosphere and increases to more than 4 years in the extratropical lower stratosphere (Andrews et al., 2001; Waugh and Hall, 2002). Thus, perturbations of stratospheric flow can be expected to have a delayed response to perturbations in surface fluxes.

Figure S16 is comparable to Fig. 17 but for the in situ-based fluxes. As with GOSAT data, seasonal variation in

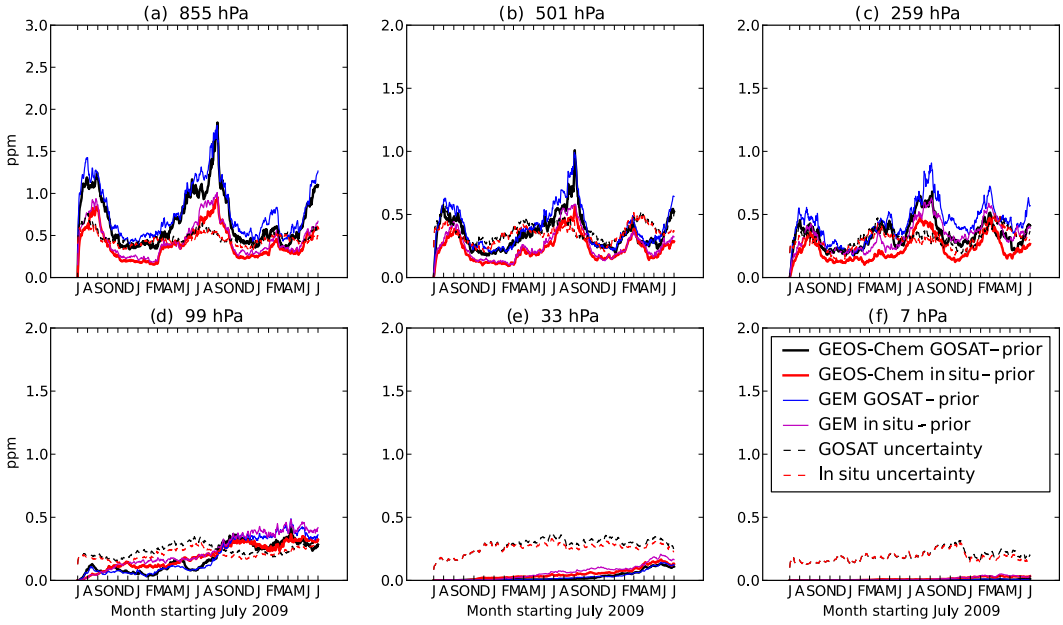

Figure 18. Global mean of the zonal standard deviation of the CO_2 PAAF for 1 July 2009 to 30 June 2011 from the GOSAT-based posterior fluxes (solid black curves) and the in situ-based posterior fluxes (solid red curves). PAAFs are shown for the model level closest to the nominal pressure level indicated above each panel for both GEOS-Chem (thick lines) and GEM-MACH-GHG (thin lines). The zonal standard deviation of the CO_2 uncertainty is shown for the GOSAT posterior flux integration (black dashed curves) and the in situ posterior flux integration (red dashed curves). Uncertainty in CO_2 is estimated with GEM-MACH-GHG by perturbing the meteorological analyses and computing the difference in CO_2 from the unperturbed integration with a given set of posterior fluxes.

PAAF is also seen in the lower and middle troposphere in the northern extratropics. There is also a seasonal variation in the zonal standard deviations in the tropics (Fig. S16a–b). Spatial variations in the tropics are larger in boreal summer as well as in March 2011. The March 2011 event was also seen with GOSAT data and with both models (Fig. 19f) and may be related to the fact that enhanced CO_2 in tropical Asia was seen in commercial-aircraft-based in situ data in March to May 2011 (Basu et al., 2014, their Fig. 3). As with the GOSAT-based PAAF, the magnitude of zonal standard deviations diminishes with altitude, and in the stratosphere, a trend in values is seen (Fig. S16d–e). The differences in zonal asymmetry of PAAF seen with the two observing systems are directly compared in Fig. 18. Now it is clear that more zonal structure is apparent with GOSAT data in the lower and middle troposphere (Fig. 18a–b). Also, the slightly greater zonal structure in stratospheric increments obtained with in situ data in the first year is also evident (Fig. 18d). However, the PAAF in the stratosphere due to the assimilation of observations does not exceed that due to wind field uncertainty in the middle and upper stratosphere (Fig. 18e–f). In the lower stratosphere (Fig. 18d), the zonal structure in the first year is also not to be trusted in our inversion. In the lower troposphere, zonal asymmetry in GOSAT PAAFs exceeds that arising from wind field uncertainty except in November, December and January (Fig. 18a). However, in our inversion, for in situ data, the zonal structure can only be trusted in boreal summer (June, July and August). Thus, based on both models and the same prior flux, the satellite data are potentially able to retrieve fluxes on finer spatial scales than are in situ data through most of the year, but it is important to note that more spatial structure does not mean correct spatial structure. Validation of spatial structures in posterior distributions needs to be made against a dense network of independent observations in order to determine if the increased spatial variation is correct. Given the difference in observation densities (Figs. 1 and 2), this result is not surprising. The lack of ability of in situ data to produce zonal asymmetry in posterior atmospheric adjustments (PAAFs) that are larger than those arising from uncertainty in wind fields (PAAMs) outside of boreal summer seen here may indicate why it has been difficult for flux inversions to regionally attribute sources with this observation network (e.g. Gurney et al., 2002; Peters et al., 2010; Bruhwiler et al., 2011; Peylin et al., 2013).

Contributions of the three zonal bands to the globally averaged zonal standard deviations are shown in Fig. 19. In the northern extratropics, GOSAT data produce zonal structures that exceed errors due to wind field uncertainty from May to October in the lower troposphere (Fig. 19a), from June to September in the middle troposphere (Fig. 19b) and in July and August in the upper troposphere (Fig. 19c). However, the in situ data produce zonal structures that do not exceed meteorological uncertainty levels except in July, August and September in the lower troposphere (Fig. 19a). In

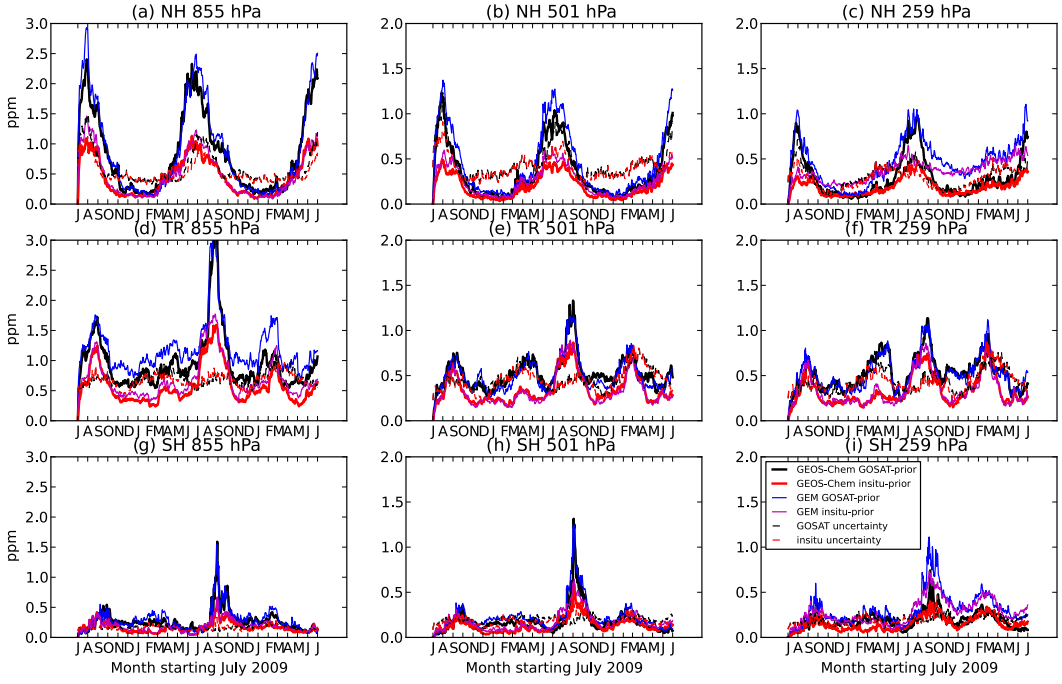

Figure 19. Regional contributions to the global mean of the zonal standard deviation of the CO_2 PAAF for 1 July 2009 to 30 June 2011 from the GOSAT-based posterior fluxes (solid black curves) and the in situ-based posterior fluxes (solid red curves). PAAFs are shown for the model level closest to the nominal pressure level indicated above each panel for both GEOS-Chem (thick lines) and GEM-MACH-GHG (thin lines). Regional contributions have been multiplied by a factor of 3 as in Fig. 14. Uncertainty in zonal standard deviation of CO_2 is shown for the GOSAT posterior flux integration (dashed cyan curves) and the in situ posterior flux integration (dashed magenta curves). Uncertainty in CO_2 is estimated for each integration by perturbing the meteorological analyses and computing the difference from the unperturbed integration.

the tropics, zonal structure is evident in CO_2 fields forced by GOSAT posterior fluxes in the lower troposphere at all times (Fig. 19d). In the middle troposphere, the tropical zonal structure exceeds meteorological uncertainty levels in August, September and October (Fig. 19e). For the CO_2 fields informed by in situ observations, the zonal structure in the tropics exceeds this level only in July, August and September in the lower and middle troposphere (Fig. 19d–e). In August and September 2010, in the upper troposphere (Fig. 19f), both GOSAT and in situ data produce zonal structure that exceeds that arising from uncertain wind fields. Both models also produce qualitatively similar results with the exception of the tropical lower troposphere (Fig. 19d) and the UTLS region in the second year (Fig. 19c, i) where GEM-MACH-GHG produces more zonal structure. Given the much higher resolution (horizontally and vertically) of this model, it can generate finer-scale structures from the coarse-resolution fluxes that eventually propagate to the stratosphere. The differences may also be due to the higher resolution of GEM-MACH-GHG directly producing spatial variations in UTLS flow and in the tropics.

In this subsection, the zonal standard deviations of the PAAF were examined in a global sense and in terms of contributions to the global values. The same prior flux was used in both inversions. For this choice of prior flux, the potential benefit of the higher density GOSAT observations is clearly evident in enhanced zonal structures, particularly in the northern extratropics in boreal summer and in the tropics, year-round. These values exceed the uncertainty in CO_2 due to uncertain meteorology much of the time. However, these diagnostics can only indicate a potential benefit since the increased zonal variation was not validated against independent measurements. While this type of validation is not yet possible because it requires high-resolution, globally distributed, independent measurement networks, Houweling et al. (2015) found that flux inversions with GOSAT data do not agree with each other on subcontinental scales. They conclude that flux inversions using GOSAT data do not sufficiently constrain regional-scale fluxes.

4 Summary and discussion

The results from flux inversion analyses are difficult to verify due to the lack of a dense, global network of flux measurements. In this work, we demonstrate that it is possible to glean useful information about flux inversion results by looking at the changes made to the tracer fields. The data

assimilation process yields updates to prior fluxes, or "flux increments", but here we consider the tracer field increment. This increment is denoted the posterior atmospheric adjustment (PAA) and refers to the change in concentrations obtained from a model integration using posterior fluxes, initial states and wind fields relative to those from another integration using prior fluxes, initial states and wind fields. We show that there are many components to the PAA and consider two of these: posterior atmospheric adjustments due to fluxes (PAAF) and those due to meteorological uncertainty (PAAM). By comparing PAAF and PAAM, we obtain a new diagnostic for assessing retrieved fluxes. Specifically, when PAAF exceeds PAAM, atmospheric changes due to fluxes exceed those due to random perturbations in meteorological fields and should be more thoroughly verified against independent measurements. When this does not occur, PAAF is not robust against some types of transport error (namely, that due to imperfect meteorology). This information will be useful for inverse model intercomparisons. The diagnostic could also be extended to check that PAAF also exceeds adjustments arising from initial condition updates.

Although our new diagnostic depends on the model and prior fluxes used, as is always the case with diagnostics based on analysis increments, we demonstrate its utility by comparing flux inversion results obtained with the GEOS-Chem 4D-Var system and two different observing systems: in situ (Deng et al., 2014) and GOSAT (Deng et al., 2016). The largest contribution to the global PAAF in the troposphere is from the northern extratropics but the stratospheric signal primarily reflects tropical influence (Fig. 15). The global PAAF due to GOSAT observations has much stronger seasonal variations than that due to in situ observations (Fig. 14). Furthermore, a difference of about 0.5 ppm is seen between the simulations obtained using GOSAT and in situ posterior fluxes, with the latter agreeing better with observations (TCCON, HIPPO-3 in the northern extratropics above the middle troposphere and NOAA aircraft on annual timescales) (Figs. 9, 11, S10, S12, S13). The inversion constrained by GOSAT data does not recover the global mean flux as well as the in situ inversion on these long timescales. However, GOSAT-informed CO_2 distributions can be revealed to better capture the seasonal cycle at most northern extratropical TCCON sites (Figs. 10, S11). Zonal standard deviations of the PAAF (which reveal spatial structures in the zonal direction) are much larger when GOSAT-informed posteriors are used (in the northern extratropics outside of boreal winter and in the tropics throughout the year) (Figs. 17, 18).

Since the PAAF depends on the transport model used, we used two different models (GEOS-Chem and GEM-MACH-GHG) to define the PAAF. Since GEOS-Chem was used for the flux inversions, subsequent integrations of posterior fluxes are consistent with the transport assumed during the flux inversion. However, the posterior CO_2 distributions obtained with GEM-MACH-GHG convolve its transport model error with that of GEOS-Chem. Indeed, a difference in model transport times to the Southern Hemisphere was seen. Yet despite this caveat, all of the main conclusions held for both models. Moreover, the use of GEM-MACH-GHG, which is a coupled meteorology-tracer transport model, permitted the calculation of uncertainties in posterior CO_2 distributions due to uncertain wind fields (PAAM). Actual meteorological analysis errors were used to perturb wind fields and repeat all simulations (see Supplement). The impact of perturbed wind fields on CO_2 distributions was used to define a minimum level of uncertainty (since in reality, model integrations of CO_2 will also include errors from fluxes, model formulation and representativeness as well as the inevitable imperfections from meteorological analyses). This error was useful for determining when spatial scales (characterized by departures from zonal means) are robust against transport error arising from meteorological uncertainty although, being a minimum error, it provides an optimistic assessment. In situ observations were found to generate zonal standard deviations larger than this minimum level only in boreal summer, whereas GOSAT data exceeded this threshold through most of the year (Figs. 18, 19). This potential for retrieving finer spatial scales with GOSAT sampling relative to the in situ network makes sense given the density of GOSAT observations (Fig. 2) and is consistent with the prediction of Takagi et al. (2014) or Deng et al. (2016). Moreover, the increased zonal structure is evident throughout the year in the tropics and in all seasons except boreal winter in the northern extratropics is rather encouraging. However, verifying such finer scales will be challenging given the limited spatial coverage of validating measurements from TCCON or aircraft platforms and temporal and spatial scales resolved may depend on the characteristics of the flux inversion system. Indeed, the current dispute over the enhanced European sinks obtained with GOSAT data (Feng et al., 2016; Reuter et al., 2014; Houweling et al., 2015) indicates that the finer spatial scales retrieved are not necessarily correct and are difficult to validate. It is plausible that spurious zonal structures in the PAAF could be introduced by spatially varying biases in the observations or uneven spatial coverage. However, there is also evidence supporting the ability of space-based observations to recover zonal asymmetries in the CO_2 fields. Liu et al. (2017) use observations from GOSAT and OCO-2 to isolate tropical flux anomalies between continents during the 2015–2016 El Niño event, while Chatterjee et al. (2017) found that zonal asymmetries in XCO_2 anomalies could be isolated during the same El Niño event. Because our uncertainty arises from imperfect meteorological analyses, its impact cannot be seen in flux inversions obtained from a single model forced by a single set of driving meteorological fields. However, this error source should be present in multi-system comparison studies when the systems use different sources of meteorological fields.

By examining the behaviour of each observing system separately, it was possible to isolate differences in their impact on posterior fluxes obtained with our flux inversion system.

In particular, it is found that the in situ observing system results in posterior fluxes that well define the global mean CO_2 on annual timescales and that there is a dependence of seasonal variations of the global PAAF on the observation system. However, both systems defined the annual budget for 2010 equally well. The importance of these results is twofold. First, the implications are that caution should be exercised when drawing conclusions based on sub-annual variations of the global mean CO_2 because they depend on the observation sets used. Since CO_2 has strong seasonal variations, the PAAF in the lower atmosphere should also have seasonal variations if the prior fluxes have errors on seasonal timescales (e.g. as in Liu et al., 2014, or Ott et al., 2015). The challenge is that the seasonal variation of GOSAT data coverage will be convolved with an actual seasonal variation of fluxes. Second, our results identify temporal scales of atmospheric CO_2 that are best constrained by each observing network, in the context of our flux inversion system. Specifically, the in situ network captures global mean (and the 18-month mean at most TCCON stations) well, while GOSAT better captures the seasonal cycle at northern extratropical TCCON sites. Understanding the timescales resolved by different observing systems will be critical for the CO_2 assimilation problem with coupled meteorological and GHG transport models at operational centres which are geared toward short assimilation windows (e.g. Polavarapu et al., 2016; Agustí-Panareda et al., 2014; Massart et al., 2016; Ott et al., 2015). For such systems, long-timescale information will be challenging to extract from observations and may require novel multi-timescale analysis approaches.

While our results regarding the behaviour of each observing system may have important implications for flux estimation, they must be seen in the context of the inversion system used, namely, GEOS-Chem and 4D-Var with long assimilation windows. Aspects of the inversion system may impact the results. For this reason, repetition of our experiments with other inversion systems is desirable to determine the generality of results across inversion systems. Furthermore, we suggest that comparing PAAFs obtained by integrating a single model with known transport behaviour with posterior fluxes from various different inversion systems could be a useful diagnostic because it will identify relative mismatches of transport times between models. For example, CT2013B fluxes with our weather model (GEM-MACH-GHG) identified a mismatch in transport of mid-latitude fluxes in boreal summer to the high Arctic in autumn with TM5 (Polavarapu et al., 2016) as well as a too-fast transport of GEOS-Chem from the tropics to the Southern Hemisphere relative to GEM-MACH-GHG. While this diagnostic cannot determine which model's transport is correct, if the reference model's transport issues were known (from age-of-air diagnostics, for example), the PAAF comparison offers a fast, simple way to infer transport issues of other models. However, only obvious transport mismatches would be identifiable. Regional-scale or shorter timescale transport mismatches would be hard to identify with a sparse verifying observation network. Indeed, as a result of this work, we plan to identify GEM-MACH-GHG's transport issues through age-of-air diagnostics in the future.

In addition to the dependence of the diagnostic on the transport model, and the inversion system used to generate posterior fluxes, the dependence on the choice of prior fluxes is also worth noting. Since we used the same prior fluxes for both sets of inversions, PAAFs could be compared and this yielded the insights noted above. However, the choice of prior flux impacts comparisons of PAAF to PAAM. For example, with a very realistic prior flux, the observations will have little room to improve fluxes during the flux inversion so that PAAFs could be small. Then comparison to PAAM may reveal that posterior fluxes do not change atmospheric tracer distributions more significantly than meteorological uncertainty does. In that case, the given assimilation system is limited by meteorological uncertainty. Further improvements could be obtained with more accurate or dense observations (to increase PAAF) or by reducing meteorological uncertainty (to decrease PAAM). Thus, the system dependence of the diagnostic can be useful for monitoring the behaviour of an assimilation system over time.

Although only in situ and GOSAT-based flux inversions were considered here, it is natural to wonder if the results would apply to OCO-2. Byrne et al. (2017) note that OCO-2 has higher spatial resolution and higher precision (due to aggregation of measurements in 2×2.5 grid) and that OCO-2 is better at picking up NH extratropical fluxes than GOSAT (their Fig. 10). OCO-2 also had the best constraints on regional fluxes in the tropics. It is easy to speculate that even finer spatial scales than seen here with GOSAT data could be expected to exceed meteorological uncertainties. However, OCO-2 also has a seasonal variation in coverage which has been shown to produce a bias in global annual flux (Liu et al., 2014). Although Liu et al. (2014), and Houweling et al. (2015) suggest that flux inversion systems are partly to blame by not permitting seasonal correlations of error covariances, it may be desirable to obtain additional measurements of the Northern Hemisphere during boreal winter. GOSAT, OCO-2 and TanSat measure in the shortwave infrared range so their latitudinal coverage does vary seasonally. The seasonal variation of coverage could be reduced if more nadir observations over snow-covered regions were processed for the winter or more ocean glint observations were made in winter. (However, signal-to-noise ratio for the CO_2 bands is lower over snow, so retrieving over snow will typically result in poorer precision than over other surfaces.) Furthermore, active measurements such as Active Sensing of CO_2 Emissions over Nights, Days and Seasons (ASCENDS) (https://fpd.larc.nasa.gov/ascends.html, last access: 7 August 2018) that do not depend on sunlight would complement the current network of in situ and satellite measurements.

In this work, we have separately considered the impact of in situ and GOSAT data on posterior CO_2 distributions in or-

der to better understand the behaviour of each type of observation in the context of a flux inversion and modelling system. Ultimately, the best network will be a combination of both types of observation (Baker et al., 2006). By revealing the complementary benefits of the two types of observations, our results indicate a need for further research to understand how best to adapt flux inversion systems to take advantage of each type of observation. For example, in situ data could constrain biases in satellite data as in Feng et al. (2016) but perhaps also the long-timescale global mean, with satellite data being used to improve regional-scale fluxes. We have also separately considered the impacts of flux increments and meteorological uncertainties on tracer adjustments from prior distributions. However, meteorological uncertainty is only one component of transport error (Polavarapu et al., 2016, Sect. 2). Thus, we are developing a coupled meteorological, constituent and flux estimation system using GEM-MACH-GHG within an ensemble Kalman filter. With this system we will be able to quantify transport error by simulating all of its components (flux errors, meteorological errors, initial state errors and model errors) and extend the analysis begun here. For example, fully 4-dimensional transport error standard deviations sampled at observing sites can be used to compare errors from column and surface measurements and to determine whether column measurements are really less sensitive to transport errors. The covariation of transport error and CO_2 variation along weather fronts can also be assessed.

Data availability. The GEM model codes which were used in this work (version 4.8-LTS.13) are available at https://github.com/armnlib (last access: 7 August 2018). These source codes are copyrighted but are available subject to the GNU Lesser General Public License (LGPL v2.1) agreement. Some documentation on GEM is available at http://collaboration.cmc.ec.gc.ca/science/rpn/gem/gemdm/gemdm.html (last access: 7 August 2018) and http://collaboration.cmc.ec.gc.ca/science/rpn/gef_html_public/ (last access: 7 August 2018). The GEM-MACH source code is available upon request to michael.neish@canada.ca, and is subject to the LGPL v2.1 license. ECCC's model output data are available at https://weather.gc.ca/grib/index_e.html (last access: 7 August 2018). The GEOS-Chem model, including the adjoint code, is freely available to the public and is distributed through GitLab. Instructions for obtaining and running the model are available on the GEOS-Chem wiki: http://wiki.seas.harvard.edu/geos-chem/ (last access: 7 August 2018). The in situ observations used in the GEOS-Chem inversions are available from ftp://ftp.cmdl.noaa.gov/data/trace_gases/co2/flask/surface/ (last access: 7 August 2018). The GOSAT level 2 ACOS b3.4 data were obtained from http://co2.jpl.nasa.gov (last access: 7 August 2018). The TCCON, HIPPO-3 and NOAA aircraft observations used for validation are available from https://tccondata.org (last access: 7 August 2018), https://hippo.ornl.gov (last access: 7 August 2018) and https://doi.org/10.3334/OBSPACK/1001 (last access: 7 August 2018), respectively.

Appendix A

The GEOS-Chem adjoint model (Henze et al., 2007) calculates the derivative of the modelled CO_2 concentration with respect to a set of model parameters, f. We use the adjoint model to calculate the sensitivity of modelled CO_2 concentrations to an earlier atmospheric CO_2 state over a volume of atmosphere with units of parts per million by volume (ppm) and use the adjoint model to calculate the gradient $\nabla_f J$. For this study, J is defined as the mean CO_2 concentration over 20° S–20° N and 500–250 hPa at instantaneous time t_0:

$$J = \left[\sum_{k=500\,\mathrm{hPa}}^{250\,\mathrm{hPa}} \sum_{j=-20^\circ}^{20^\circ} \sum_{i=0^\circ}^{360^\circ} \frac{C_{i,j,k,t_0}}{M_{i,j,k,t_0}} \right] \times 10^6, \tag{A1}$$

where C_{i,j,k,t_0} and M_{i,j,k,t_0} are the molar abundances of CO_2 and air at longitude i, latitude j, level k and time t_0. Gas abundances are obtained by sampling a forward model simulation at the time t_0. The sensitivity is obtained by calculating the gradient of J with respect to an earlier atmospheric CO_2 state, $f_{i,j,k,t}$:

$$\gamma_{i,j,k,t} = \frac{\partial J}{\partial f_{i,j,k,t}}. \tag{A2}$$

The Supplement related to this article is available online at https://doi.org/10.5194/acp-18-12011-2018-supplement.

Author contributions. SMP designed and performed the experiments with GEM-MACH-GHG. FD performed the GEOS-Chem flux inversion experiments and the comparisons of both model outputs to TCCON and HIPPO data. BB performed the adjoint sensitivity experiments. DBAJ provided important input into interpretation of the results. MN assisted with the GEM-MACH-GHG model development and diagnosing experiments and wrote or contributed to most of the diagnostics. SMP wrote the paper with contributions from all other co-authors.

Competing interests. The authors declare that they have no conflict of interest.

Special issue statement. This article is part of the special issue "The 10th International Carbon Dioxide Conference (ICDC10) and the 19th WMO/IAEA Meeting on Carbon Dioxide, other Greenhouse Gases and Related Measurement Techniques (GGMT-2017) (AMT/ACP/BG/CP/ESD inter-journal SI)". It is a result of the 10th International Carbon Dioxide Conference, Interlaken, Switzerland, 21–25 August 2017.

Acknowledgements. Work at the University of Toronto was supported by funding from the Canadian Space Agency, Environment and Climate Change Canada, and the Natural Science and Engineering Research Council of Canada. We are grateful to Ray Nassar and Douglas Chan for helpful comments on an earlier version of this paper. ACOS GOSAT data were produced by the ACOS/OCO-2 project at the Jet Propulsion Laboratory (JPL), California Institute of Technology, and obtained from the JPL website, http://co2.jpl.nasa.gov (last access: 7 August 2018). We acknowledge the GOSAT Project for acquiring these spectra. TCCON data were obtained from the TCCON Data Archive, hosted by the Carbon Dioxide Information Analysis Center (CDIAC) at https://tccondata.org (last access: 7 August 2018). We thank TCCON PIs Paul Wennberg, Caltech (Lamont, Park Falls); David Griffith, University of Wollongong (Darwin and Wollongong); Justus Notholt, University of Bremen (Bremen); Nicholas Deutscher, University of Bremen (Białystok); Thorsten Warneke, University of Bremen (Orléans); Dave Pollard, NIWA (Lauder); Ralf Sussmann, IMKIFU (Garmisch); Kimberly Strong, University of Toronto (Eureka); Rigel Kivi, FMI (Sodankylä); Frank Hase, KIT (Karlsruhe); and Matthias Schneider, KIT (Izaña). We are grateful to Colm Sweeney (NOAA ESRL) for providing the NOAA aircraft profiles and to Ken Masarie of the NOAA Global Monitoring Division in Boulder, Colorado for compiling ObsPack2013. The National Oceanic and Atmospheric Administration (NOAA) North American Carbon Program has funded NOAA/ESRL Global Greenhouse Gas Reference Network Aircraft program. The ObsPack data were obtained for the period 2000–2012 (obspack_co2_1_PROTOTYPE_v1.0.4_2013-11-25) from https://doi.org/10.3334/OBSPACK/1001. We are grateful to NSF and NOAA for producing and providing HIPPO-3 (https://hippo.ornl.gov, last access: 7 August 2018) aircraft measurements (HIPPO Merged 10-second Meteorology, Atmospheric Chemistry, Aerosol Data (R_20121129)). We would like to thank Doug Worthy of Atmospheric Science and Technology Directorate (ASTD), Environment and Climate Change Canada, for developing and maintaining ECCC's greenhouse gas measurement network and for providing the CO_2 concentration measurement data.

Edited by: Rachel Law
Reviewed by: two anonymous referees

References

Agustí-Panareda, A., Massart, S., Chevallier, F., Boussetta, S., Balsamo, G., Beljaars, A., Ciais, P., Deutscher, N. M., Engelen, R., Jones, L., Kivi, R., Paris, J.-D., Peuch, V.-H., Sherlock, V., Vermeulen, A. T., Wennberg, P. O., and Wunch, D.: Forecasting global atmospheric CO_2, Atmos. Chem. Phys., 14, 11959–11983, https://doi.org/10.5194/acp-14-11959-2014, 2014.

Andres, R. J., Gregg, J. S., Losey, L., Marland, G., and Boden, T. A.: Monthly, global emissions of carbon dioxide from fossil fuel consumption, Tellus B, 63, 309–327, https://doi.org/10.1111/j.1600-0889.2011.00530.x, 2011.

Andrews, A. E., Boering, K. A., Daube, B. C., Wofsy, S. C., Loewenstein, M., Jost, H., Podolske, J. R., Webster, C. R., Herman, R. L., Scott, D. C., Flesch, G. J., Moyer, E. J., Elkins, J. W., Dutton, G. S., Hurst, D. F., Moore, F. L., Ray, E. A., Romashkin, P. A., and Strahan, S. E.:, Mean ages of stratospheric air derived from in situ observations of CO_2, CH_4, and N_2O, J. Geophys. Res., 106, 32295–32314, https://doi.org/10.1029/2001JD000465, 2001.

Baker, D. F., Doney, S. C., and Schimel, D. S.: Variational data assimilation for atmospheric CO_2, Tellus B, 58, 359–365, 2006.

Barnes, E. A., Parazoo, N., Orbe, C., and Denning, A. S.: Isentropic transport and the seasonal cycle amplitude of CO_2, J. Geophys. Res.-Atmos., 121, 8106–8124, 2016.

Basu, S., Guerlet, S., Butz, A., Houweling, S., Hasekamp, O., Aben, I., Krummel, P., Steele, P., Langenfelds, R., Torn, M., Biraud, S., Stephens, B., Andrews, A., and Worthy, D.: Global CO_2 fluxes estimated from GOSAT retrievals of total column CO_2, Atmos. Chem. Phys., 13, 8695–8717, https://doi.org/10.5194/acp-13-8695-2013, 2013.

Basu, S., Krol, M., Butz, A., Clerbaux, C., Sawa, Y., Machida, T., Matsueda, H., Frankenberg, C., Hasekamp, O. P., and Aben, I.: The seasonal variation of the CO_2 flux over Tropical Asia estimated from GOSAT, CONTRAIL, and IASI, Geophys. Res. Lett., 41, 1809–1815, https://doi.org/10.1002/2013GL059105, 2014.

Blumenstock, T., Hase, F., Schneider, M., García, O. E., and Sepúlveda, E.: TCCON data from Izana, Tenerife, Spain, Release GGG2014R0, TCCON data archive, Carbon Dioxide Information Analysis Center, Oak Ridge National Laboratory, Oak Ridge, Tennessee, USA, https://doi.org/10.14291/tccon.ggg2014.izana01.R0/1149295, 2014.

Bruhwiler, L. M. P., Michalak, A. M., and Tans, P. P.: Spatial and temporal resolution of carbon flux estimates for 1983–2002, Biogeosciences, 8, 1309–1331, https://doi.org/10.5194/bg-8-1309-2011, 2011.

Butz, A., Guerlet, S., Hasekamp, O., Schepers, D., Galli, A., Aben, I., Frankenbert, C. F., Hartmann, J.-M., Tran, H., Kuze, A., Keppel-Aleks, G., Toon, G., Wunch, D., Wennberg, P., Deutscher, N., Griffith, D. G., Macatangay, R., Messerschmidt, J., Notholt, J., and Warneke, T.: Toward accurate CO_2 and CH_4 observations from GOSAT, Geophys. Res. Lett., 38, L14812, https://doi.org/10.1029/2011GL047888, 2011.

Byrne, B. D., Jones, B. A., Strong, K., Zeng, Z.-C., Deng, F., and Liu, J.: Sensitivity of CO_2 surface flux constraints to observational coverage, J. Geophys. Res.-Atmos., 122, 6672–6694, https://doi.org/10.1002/2016JD026164, 2017.

Chatterjee, A., Gierach, M. M., Sutton, A. J., Feely, R. A., Crisp, D., Eldering, A., Gunson, M. R., O'Dell, C. W., Stephens, B. B., and Schimel, D. S.: Influence of El Niño on atmospheric CO_2 over the tropical Pacific Ocean: Findings from NASA's OCO-2 mission, Science, 358, eaam5776, https://doi.org/10.1126/science.aam5776, 2017.

Chen, J. M., Mo, G., Pisek, J., Liu, J., Deng, F., Ishizawa, M., and Chan, D.: Effects of foliage clumping on the estimation of global terrestrial gross primary productivity, Global Biogeochem. Cy., 26, GB1019, https://doi.org/10.1029/2010gb003996, 2012.

Chevallier, F., Feng, L., Bösch, H., Palmer, P. I., and Rayner: On the impact of transport model errors for the estimation of CO_2 surface fluxes from GOSAT observations, Geophys. Res. Lett., 37, L21803, https://doi.org/10.1029/2010GL044652, 2010.

Chevallier, F., Palmer, P. I., Feng, L., Boesch, H., O'Dell, C. W., and Bousquet, P.: Toward robust and consistent regional CO_2 flux estimates from in situ and spaceborne measurements of atmospheric CO_2, Geophys. Res. Lett., 41, 1065–1070, https://doi.org/10.1002/2013GL058772, 2014.

Ciais, P., Sabine, C., Bala, G., Bopp, L., Brovkin, V., Canadell, J., Chhabra, A., DeFries, R., Galloway, J., Heimann, M., Jones, C., Le Quéré, C., Myneni, R. B., Piao S., and Thornton, P.: Carbon and Other Biogeochemical Cycles, in: Climate Change 2013: The Physical Science Basis. Contribution of Working Group I to the Fifth Assessment Report of the Intergovernmental Panel on Climate Change, edited by: Stocker, T. F., Qin, D., Plattner, G.-K., Tignor, M., Allen, S. K., Boschung, J., Nauels, A., Xia, Y., Bex, V., and Midgley, P. M., Cambridge University Press, Cambridge, UK and New York, NY, USA, 2013.

Conway, T. J. and Tans, P. P.: Trends in atmospheric carbon dioxide, available at: http://www.esrl.noaa.gov/gmd/ccgg/trends, last access: April 2012.

Conway, T. J., Lang, P. M., and Masarie, K. A.: Atmospheric Carbon Dioxide Dry Air Mole Fractions from the NOAA ESRL Carbon Cycle Cooperative Global Air Sampling Network, 1968–2010, Version: 2011-10-14, available at: ftp://ftp.cmdl.noaa.gov/data/trace_gases/co2/flask/surface/ (last access: 7 August 2018), 2011.

Corbett, J. J.: Considering alternative input parameters in an activity-based ship fuel consumption and emissions model: Reply to comment by Øyvind Endresen et al. on "Updated emissions from ocean shipping", J. Geophys. Res., 109, D23303, https://doi.org/10.1029/2004jd005030, 2004.

Corbett, J. J. and Koehler, H. W.: Updated emissions from ocean shipping, J. Geophys. Res., 108, 4650–4666, https://doi.org/10.1029/2003jd003751, 2003.

Corbin, K. D., Denning, A. S., and Parazoo, N. C.: Assessing temporal clear-sky errors in assimilation of satellite CO_2 retrievals using a global transport model, Atmos. Chem. Phys., 9, 3043–3048, https://doi.org/10.5194/acp-9-3043-2009, 2009.

Crisp, D. and OCO-2 Science Team: Measuring Atmospheric Carbon Dioxide from Space with the Orbiting Carbon Observatory-2 (OCO-2), Proc. SPIE 9607, Earth Observing Systems XX, 960702, https://doi.org/10.1117/12.2187291, 2015.

Crisp, D., Pollock, H. R., Rosenberg, R., Chapsky, L., Lee, R. A. M., Oyafuso, F. A., Frankenberg, C., O'Dell, C. W., Bruegge, C. J., Doran, G. B., Eldering, A., Fisher, B. M., Fu, D., Gunson, M. R., Mandrake, L., Osterman, G. B., Schwandner, F. M., Sun, K., Taylor, T. E., Wennberg, P. O., and Wunch, D.: The on-orbit performance of the Orbiting Carbon Observatory-2 (OCO-2) instrument and its radiometrically calibrated products, Atmos. Meas. Tech., 10, 59–81, https://doi.org/10.5194/amt-10-59-2017, 2017.

Deng, F. and Chen, J. M.: Recent global CO_2 flux inferred from atmospheric CO_2 observations and its regional analyses, Biogeosciences, 8, 3263–3281, https://doi.org/10.5194/bg-8-3263-2011, 2011.

Deng, F., Chen, J. M., Plummer, S., Chen, M. Z., and Pisek, J.: Algorithm for global leaf area index retrieval using satellite imagery, IEEE T. Geosci. Remote, 44, 2219–2229, https://doi.org/10.1109/tgrs.2006.872100, 2006.

Deng, F., Jones, D. B. A., Henze, D. K., Bousserez, N., Bowman, K. W., Fisher, J. B., Nassar, R., O'Dell, C., Wunch, D., Wennberg, P. O., Kort, E. A., Wofsy, S. C., Blumenstock, T., Deutscher, N. M., Griffith, D. W. T., Hase, F., Heikkinen, P., Sherlock, V., Strong, K., Sussmann, R., and Warneke, T.: Inferring regional sources and sinks of atmospheric CO_2 from GOSAT XCO_2 data, Atmos. Chem. Phys., 14, 3703–3727, https://doi.org/10.5194/acp-14-3703-2014, 2014.

Deng, F., Jones, D. B. A., Walker, T. W., Keller, M., Bowman, K. W., Henze, D. K., Nassar, R., Kort, E. A., Wofsy, S. C., Walker, K. A., Bourassa, A. E., and Degenstein, D. A.: Sensitivity analysis of the potential impact of discrepancies in stratosphere–troposphere exchange on inferred sources and sinks of CO_2, Atmos. Chem. Phys., 15, 11773–11788, https://doi.org/10.5194/acp-15-11773-2015, 2015.

Deng, F., Jones, D. B. A., O'Dell, C. W., Nassar, R., and Parazoo, N. C.: Combining GOSAT XCO_2 observations over land and ocean to improve regional CO_2 flux estimates, J. Geophys. Res.-Atmos., 121, 1896–1913, https://doi.org/10.1002/2015JD024157, 2016.

Deutscher, N., Notholt, J., Messerschmidt, J., Weinzierl, C., Warneke, T., Petri, C., Grupe, P., and Katrynski, K.: TCCON data from Bialystok, Poland, Release GGG2014R0, TCCON data archive, Carbon Dioxide Information Analysis Center, Oak Ridge National Laboratory, Oak Ridge, Tennessee, USA, https://doi.org/10.14291/tccon.ggg2014.bialystok01.R0/1149277, 2014.

Endresen, Ø., Sørgård, E., Bakke, J., and Isaksen, I. S. A.: Substantiation of a lower estimate for the bunker inventory: Comment on "Updated emissions from ocean shipping" by James J. Corbett and Horst W. Koehler, J. Geophys. Res., 109, D23302, https://doi.org/10.1029/2004jd004853, 2004.

Endresen, Ø., Sørgård, E., Behrens, H. L., Brett, P. O., and Isaksen, I. S. A.: A historical reconstruction of ships' fuel consumption and emissions, J. Geophys. Res., 112, D12301, https://doi.org/10.1029/2006jd007630, 2007.

Feng, L., Palmer, P. I., Parker, R. J., Deutscher, N. M., Feist, D. G., Kivi, R., Morino, I., and Sussmann, R.: Estimates of European uptake of CO_2 inferred from GOSAT XCO_2 retrievals: sensitivity to measurement bias inside and outside Europe, Atmos. Chem. Phys., 16, 1289–1302, https://doi.org/10.5194/acp-16-1289-2016, 2016.

Friedl, R. R.: Atmospheric effects of subsonic aircraft: interim assessment report of the Advanced Subsonic Technology Program, p. 168, National Aeronautics and Space Administration, Goddard Space Flight Center, Greenbelt, MD United States, 1997.

Griffith, D. W. T., Deutscher, N., Velazco, V. A., Wennberg, P. O., Yavin, Y., Aleks, G. K., Washenfelder, R., Toon, G. C., Blavier, J.-F., Murphy, C., Jones, N., Kettlewell, G., Connor, B., Macatangay, R., Roehl, C., Ryczek, M., Glowacki, J., Culgan, T., and Bryant, G.: TCCON data from Darwin, Australia, Release GGG2014R0, TCCON data archive, Carbon Dioxide Information Analysis Center, Oak Ridge National Laboratory, Oak Ridge, Tennessee, USA, https://doi.org/10.14291/tccon.ggg2014.darwin01.R0/1149290, 2014a.

Griffith, D. W. T., Velazco, V. A., Deutscher, N., Murphy, C., Jones, N., Wilson, S., Macatangay, R., Kettlewell, G., Buchholz, R. R., and Riggenbach, M.: TCCON data from Wollongong, Australia, Release GGG2014R0, TCCON data archive, Carbon Dioxide Information Analysis Center, Oak Ridge National Laboratory, Oak Ridge, Tennessee, USA, https://doi.org/10.14291/tccon.ggg2014.wollongong01.R0/1149291, 2014b.

Gurney, K. R., Law, R. M., Denning, A. S., Rayner, P. J., Baker, D., Bousquet, P., Bruhwiler, L., Chen, Y.-H., Ciais, P., Fan, S., Fung, I. Y., Gloor, M., Heimann, M., Higuchi, K., John, J., Maki, T., Maksyutov, S., Masarle, K., Peylin, P., Prather, M., Pak, B. C., Randerson, J., Sarmiento, J., Taguchi, S., Takahashi, T., and Yuen, C.-W.: Towards robust regional estimates of CO_2 sources and sinks using atmospheric transport models, Nature, 415, 626–630, 2002.

Gurney, K. R., Law, R. M., Denning, A. S., Rayner, P. J., Baker, D., Bousquet, P., Bruhwiler, L., Chen, Y.-H., Ciais, P., Fan, S., Fung, I. Y., Gloor, M., Heimann, M., Higuchi, K., John, J., Kowalczyk, E., Maki, T., Maksyutov, S., Peylin, P., Prather, M., Pak, B. C., Sarmiento, J., Taguchi, S., Takahashi, T., and Yuen C.-W.: TransCom 3 CO_2 inversion intercomparison: 1. Annual mean control results and sensitivity to transport and prior flux information, Tellus B, 55, 555–579, 2003.

Hase, F., Blumenstock, T., Dohe, S., Groß, J., and Kiel, M.: TCCON data from Karlsruhe, Germany, Release GGG2014R1, TCCON data archive, Carbon Dioxide Information Analysis Center, Oak Ridge National Laboratory, Oak Ridge, Tennessee, USA, https://doi.org/10.14291/tccon.ggg2014.karlsruhe01.R1/1182416, 2014.

Henze, D. K., Hakami, A., and Seinfeld, J. H.: Development of the adjoint of GEOS-Chem, Atmos. Chem. Phys., 7, 2413–2433, https://doi.org/10.5194/acp-7-2413-2007, 2007.

Houtekamer, P. L., Deng, X., Mitchell, H. L., Baek, S.-J., and Gagnon, N.: Higher Resolution in an Operational Ensemble Kalman Filter, Mon. Weather Rev., 142, 1143–1162, 2014.

Houweling, S., Aben, I., Breon, F.-M., Chevallier, F., Deutscher, N., Engelen, R., Gerbig, C., Griffith, D., Hungershoefer, K., Macatangay, R., Marshall, J., Notholt, J., Peters, W., and Serrar, S.: The importance of transport model uncertainties for the estimation of CO_2 sources and sinks using satellite measurements, Atmos. Chem. Phys., 10, 9981–9992, https://doi.org/10.5194/acp-10-9981-2010, 2010.

Houweling, S., Baker, D., Basu, S. Boesch, H., Butz, A., Chevallier, F., Deng, F., Dlugokencky, E. J., Feng, L., Ganshin, A., Hasekamp, O., Jones, D., Maksyutov, S., Marshall, J., Oda, T., O'Dell, C. W., Oshchepkov, S., Palmer, P. I., Peylin, P., Poussi, Z., Reum, F., Takagi, H., Yoshida, Y., and Zhuravlev, R.: An intercomparison of inverse models for estimating sources and sinks of CO_2 using GOSAT measurements, J. Geophys. Res.-Atmos., 120, 5253–5266, https://doi.org/10.1002/2014JD022962, 2015.

Kain, J. S.: The Kain-Fritsch convective parameterization: an update, J. Appl. Meteorol. 43, 170–181, 2004.

Kain, J. S. and Fritsch, J. M.: A one-dimensional entraining/detraining plume model and its application in convective parameterizations, J. Atmos. Sci., 47, 2784–2802, 1990.

Kalnay, E., Kanamitsu, M., Kistler, R., Collins, W., Deaven, D., Gandin, L., Iredell, M., Saha, S., White, G., Woollen, J., Zhu, Y., Chelliah, M., Ebisuzaki, W., Higgins, S., Janowiak, J., Mo, K. C., Ropelewski, C., Wang, J., Leetmaa, A., Reynolds, R., Jenne, R., and Joseph, D.: The NCEP/NCAR 40-Year Reanalysis Project, B. Am. Meteorol. Soc., 77, 437–471, https://doi.org/10.1175/1520-0477(1996)077<0437:TNYRP>2.0.CO;2, 1996.

Keeling, C. D.: The concentration and isotopic abundances of carbon dioxide in the atmosphere, Tellus B, 12, 200–203, 1960.

Keppel-Aleks, G., Wennberg, P. O., and Schneider, T.: Sources of variations in total column carbon dioxide, Atmos. Chem. Phys., 11, 3581–3593, https://doi.org/10.5194/acp-11-3581-2011, 2011.

Keppel-Aleks, G., Wennberg, P. O., Washenfelder, R. A., Wunch, D., Schneider, T., Toon, G. C., Andres, R. J., Blavier, J.-F., Connor, B., Davis, K. J., Desai, A. R., Messerschmidt, J., Notholt, J., Roehl, C. M., Sherlock, V., Stephens, B. B., Vay, S. A., and Wofsy, S. C.: The imprint of surface fluxes and transport on variations in total column carbon dioxide, Biogeosciences, 9, 875–891, https://doi.org/10.5194/bg-9-875-2012, 2012.

Kim, B. Y., Fleming, G. G., Lee, J. J., Waitz, I. A., Clarke, J.-P., Balasubramanian, S., Malwitz, A., Klima, K., Locke, M., Holsclaw, C. A., Maurice, L. Q., and Gupta, M. L.: System for assessing Aviation's Global Emissions (SAGE), Part 1: Model description and inventory results, Transport Res. D-Tr. E, 12, 325–346, https://doi.org/10.1016/j.trd.2007.03.007, 2007.

Kim, J., Kim, H. M., Cho, C.-H., Boo, K.-O., Jacobson, A. R., Sasakawa, M., Machida, T., Arshinov, M., and Fedoseev, N.: Impact of Siberian observations on the optimization of surface CO_2 flux, Atmos. Chem. Phys., 17, 2881–2899, https://doi.org/10.5194/acp-17-2881-2017, 2017.

Kivi, R., Heikkinen, P., and Kyro, E.: TCCON data from Sodankyla, Finland, Release GGG2014R0, TCCON data archive, Carbon Dioxide Information Analysis Center, Oak Ridge National Laboratory, Oak Ridge, Tennessee, USA,

https://doi.org/10.14291/tccon.ggg2014.sodankyla01.R0/1149280, 2014.

Kuze, A., Suto, H., Nakajima, M., and Hamazaki, T.: Thermal and near infrared sensor for carbon observation Fourier-transform spectrometer on the Greenhouse Gases Observing Satellite for greenhouse gases monitoring, Appl. Optics, 48, 6716–6733, 2009.

Lauvaux, T. and Davis, K. J.: Planetary boundary layer errors in mesoscale inversions of column-integrated CO_2 measurements, J. Geophys. Res.-Atmos., 119, 490–508, https://doi.org/10.1002/2013JD020175, 2014.

Law, R. M., Rayner, P. J., Denning, A. S., Erickson, D., Fung, I. Y., Heimann, M., Piper, S. C., Romonet, M., Taguchi, S., Taylor, J. A., Trudinger, C. M., and Watterson, I. G.: Variations in modeled atmospheric transport of carbon dioxide and the consequences for CO_2 inversions, Global Biogeochem. Cy., 10, 783–796, 1996.

Le Quéré, C., Moriarty, R., Andrew, R. M., Canadell, J. G., Sitch, S., Korsbakken, J. I., Friedlingstein, P., Peters, G. P., Andres, R. J., Boden, T. A., Houghton, R. A., House, J. I., Keeling, R. F., Tans, P., Arneth, A., Bakker, D. C. E., Barbero, L., Bopp, L., Chang, J., Chevallier, F., Chini, L. P., Ciais, P., Fader, M., Feely, R. A., Gkritzalis, T., Harris, I., Hauck, J., Ilyina, T., Jain, A. K., Kato, E., Kitidis, V., Klein Goldewijk, K., Koven, C., Landschützer, P., Lauvset, S. K., Lefèvre, N., Lenton, A., Lima, I. D., Metzl, N., Millero, F., Munro, D. R., Murata, A., Nabel, J. E. M. S., Nakaoka, S., Nojiri, Y., O'Brien, K., Olsen, A., Ono, T., Pérez, F. F., Pfeil, B., Pierrot, D., Poulter, B., Rehder, G., Rödenbeck, C., Saito, S., Schuster, U., Schwinger, J., Séférian, R., Steinhoff, T., Stocker, B. D., Sutton, A. J., Takahashi, T., Tilbrook, B., van der Laan-Luijkx, I. T., van der Werf, G. R., van Heuven, S., Vandemark, D., Viovy, N., Wiltshire, A., Zaehle, S., and Zeng, N.: Global Carbon Budget 2015, Earth Syst. Sci. Data, 7, 349–396, https://doi.org/10.5194/essd-7-349-2015, 2015.

Lindqvist, H., O'Dell, C. W., Basu, S., Boesch, H., Chevallier, F., Deutscher, N., Feng, L., Fisher, B., Hase, F., Inoue, M., Kivi, R., Morino, I., Palmer, P. I., Parker, R., Schneider, M., Sussmann, R., and Yoshida, Y.: Does GOSAT capture the true seasonal cycle of carbon dioxide?, Atmos. Chem. Phys., 15, 13023–13040, https://doi.org/10.5194/acp-15-13023-2015, 2015.

Liu, J., Fung, I., Kalnay, E., and Kang, J.-S.: CO_2 transport uncertainties from the uncertainties in meteorological fields, Geophys. Res. Lett., 38, L12808, https://doi.org/10.1029/2011GL047213, 2011.

Liu, J., Bowman, K. W., Lee, M., Henze, D. K., Bousserez, N., Brix, H., Collatz, G. J., Menemenlis, D., Ott, L., Pawson, S., Jones, D., and Nassar, R.: Carbon monitoring system flux estimation and attribution: impact of ACOS-GOSAT XCO_2 sampling on the inference of terrestrial biospheric sources and sinks, Tellus B, 66, 1600–0889, https://doi.org/10.3402/tellusb.v66.22486, 2014.

Liu, J., Bowman, K. W., and Henze, D. K.: Source-receptor relationships of column-average CO_2 and implications for the impact of observations on flux inversions, J. Geophys. Res.-Atmos., 120, 5214–5236, https://doi.org/10.1002/2014JD022914, 2015.

Liu, J., Bowman, K. W., Schimel, D. S., Parazoo, N. C., Jiang, Z., Lee, M., Bloom, A. A., Wunch, D., Frankenberg, C., Sun, Y., O'Dell, C. W., Gurney, I. R., Menemenlis, D., Gierach, M. Crisp, D., and Eldering, A.: Contrasting carbon cycle responses of the tropical continents to the 2015–2016 El Niño, Science, 358, eaam5690, https://doi.org/10.1126/science.aam5690, 2017.

Maksyutov, S., Takagi, H., Valsala, V. K., Saito, M., Oda, T., Saeki, T., Belikov, D. A., Saito, R., Ito, A., Yoshida, Y., Morino, I., Uchino, O., Andres, R. J., and Yokota, T.: Regional CO_2 flux estimates for 2009–2010 based on GOSAT and ground-based CO_2 observations, Atmos. Chem. Phys., 13, 9351–9373, https://doi.org/10.5194/acp-13-9351-2013, 2013.

Masarie, K. A., Peters, W., Jacobson, A. R., and Tans, P. P.: ObsPack: a framework for the preparation, delivery, and attribution of atmospheric greenhouse gas measurements, Earth Syst. Sci. Data, 6, 375–384, https://doi.org/10.5194/essd-6-375-2014, 2014.

Massart, S., Agustí-Panareda, A., Heymann, J., Buchwitz, M., Chevallier, F., Reuter, M., Hilker, M., Burrows, J. P., Deutscher, N. M., Feist, D. G., Hase, F., Sussmann, R., Desmet, F., Dubey, M. K., Griffith, D. W. T., Kivi, R., Petri, C., Schneider, M., and Velazco, V. A.: Ability of the 4-D-Var analysis of the GOSAT BESD XCO_2 retrievals to characterize atmospheric CO_2 at large and synoptic scales, Atmos. Chem. Phys., 16, 1653–1671, https://doi.org/10.5194/acp-16-1653-2016, 2016.

Notholt, J., Petri, C., Warneke, T., Deutscher, N., Buschmann, M., Weinzierl, C., Macatangay, R., and Grupe, P.: TCCON data from Bremen, Germany, Release GGG2014R0. TCCON data archive, Carbon Dioxide Information Analysis Center, Oak Ridge National Laboratory, Oak Ridge, Tennessee, USA, https://doi.org/10.14291/tccon.ggg2014.bremen01.R0/1149275, 2014.

O'Dell, C. W., Connor, B., Bösch, H., O'Brien, D., Frankenberg, C., Castano, R., Christi, M., Eldering, D., Fisher, B., Gunson, M., McDuffie, J., Miller, C. E., Natraj, V., Oyafuso, F., Polonsky, I., Smyth, M., Taylor, T., Toon, G. C., Wennberg, P. O., and Wunch, D.: The ACOS CO_2 retrieval algorithm – Part 1: Description and validation against synthetic observations, Atmos. Meas. Tech., 5, 99–121, https://doi.org/10.5194/amt-5-99-2012, 2012.

Osterman, G., Eldering, A., Avis, C., O'Dell, C., Martinez, E., Crisp, D., Frankenberg, C., and Frankenberg, B.: ACOS Level 2 Standard Product version B3.4, Data User's Guide, available at: https://co2.jpl.nasa.gov/static/docs/v3.4_DataUsersGuide-RevB_131028.pdf (last access: 7 August 2018), p. 48, Jet Propulsion Laboratory, Pasadena, California, USA, 2013.

Ott, L. E., Pawson, S., Collatz, G. J., Gregg, W. W., Menemenlis, D., Brix, H., Rousseaux, C. S., Bowman, K. W., Liu, J., Eldering, A., Gunson, M. R., and Kawa, S. R.: Assessing the magnitude of CO_2 flux uncertainty in atmospheric CO_2 records using products from NASA's CarbonMonitoring Flux Pilot Project, J. Geophys. Res.-Atmos., 120, 734–765, https://doi.org/10.1002/2014JD022411, 2015.

Parazoo, N. C., Denning, A. S., Kawa, S. R., Pawson, S., and Lokupitiya, R.: CO_2 flux estimation errors associated with moist atmospheric processes, Atmos. Chem. Phys., 12, 6405–6416, https://doi.org/10.5194/acp-12-6405-2012, 2012.

Peters, W., Jacobson, A. R., Sweeney, C., Andrews, A. E., Conway, T. J., Masarie, K., Miller, J. B., Bruhwiler, L. M. P., Pétron, G., Hirsch, A. I., Worthy, D. E. J., van der Werf, G. R., Randerson, J. T., Wennberg, P. O., Krol, M. C., and Tans, P. P.: An atmospheric perspective on North American carbon dioxide exchange: CarbonTracker, P. Natl. Acad. Sci. USA, 104, 18925–18930, 2007.

Peters, W., Krol, M. C., Van Der Werf, G. R., Houweling, S., Jones, C. D., Hughes, J., Schaefer, K., Masarie, K. A., Jacob-

son, A. R., Miller, J. B., Cho, C. H., Ramonet, M., Schmidt, M., Ciattaglia, L., Apadula, F., Heltai, D., Meinhardt, F., DiSarra, A. G., Piacentino, S., Sferlazzo, D., Aalto, T., Hatakka, J., Ström, J., Haszpra, L., Meijer, H. A. J., Van der Laan, S., Neubert, R. E. M., Jordan, A., Rodó, X., Morguí, J.-A., Vermeulen, A. T., Popa, E., Rozanski, K., Zimnoch, M., Manning, A. C., Leuenberger, M., Uglietti, C., Dolman, A. J., Ciais, P., Heimann, M., and Tans, P. P.: Seven years of recent European net terrestrial carbon dioxide exchange constrained by atmospheric observations, Glob. Change Biol., 16, 1317–1337, https://doi.org/10.1111/j.1365-2486.2009.02078.x, 2010.

Peylin, P., Law, R. M., Gurney, K. R., Chevallier, F., Jacobson, A. R., Maki, T., Niwa, Y., Patra, P. K., Peters, W., Rayner, P. J., Rödenbeck, C., van der Laan-Luijkx, I. T., and Zhang, X.: Global atmospheric carbon budget: results from an ensemble of atmospheric CO_2 inversions, Biogeosciences, 10, 6699–6720, https://doi.org/10.5194/bg-10-6699-2013, 2013.

Polavarapu, S. M., Neish, M., Tanguay, M., Girard, C., de Grandpré, J., Semeniuk, K., Gravel, S., Ren, S., Roche, S., Chan, D., and Strong, K.: Greenhouse gas simulations with a coupled meteorological and transport model: the predictability of CO_2, Atmos. Chem. Phys., 16, 12005–12038, https://doi.org/10.5194/acp-16-12005-2016, 2016.

Reuter, M., Buchwitz, M., Hilker, M., Heymann, J., Schneising, O., Pillai, D., Bovensmann, H., Burrows, J. P., Bösch, H., Parker, R., Butz, A., Hasekamp, O., O'Dell, C. W., Yoshida, Y., Gerbig, C., Nehrkorn, T., Deutscher, N. M., Warneke, T., Notholt, J., Hase, F., Kivi, R., Sussmann, R., Machida, T., Matsueda, H., and Sawa, Y.: Satellite-inferred European carbon sink larger than expected, Atmos. Chem. Phys., 14, 13739–13753, https://doi.org/10.5194/acp-14-13739-2014, 2014.

Reuter, M., Buchwitz, M., Hilker, M., Heymann, J., Bovensmann, H., Burrows, J. P., Houweling, S., Liu, Y. Y., Nassar, R., Chevallier, F., Ciais, P., Marshall, J., and Reichstein, M.: How Much CO_2 Is Taken Up by the European Terrestrial Biosphere?, B. Am. Meteorol. Soc., 98, 665–671, https://doi.org/10.1175/BAMS-D-15-00310.1, 2017.

Sherlock, V. B., Connor, Robinson, J., Shiona, H., Smale, D., and Pollard, D.: TCCON data from Lauder, New Zealand, 125HR, Release GGG2014R0, TCCON data archive, Carbon Dioxide Information Analysis Center, Oak Ridge National Laboratory, Oak Ridge, Tennessee, USA, https://doi.org/10.14291/tccon.ggg2014.lauder02.R0/1149298, 2014.

Strong, K., Mendonca, J., Weaver, D., Fogal, P., Drummond, J. R., Batchelor, R., and Lindenmaier, R.: TCCON data from Eureka, Canada, Release GGG2014R0, TCCON data archive, Carbon Dioxide Information Analysis Center, Oak Ridge National Laboratory, Oak Ridge, Tennessee, USA, https://doi.org/10.14291/tccon.ggg2014.eureka01.R0/1149271, 2014.

Sussmann, R. and Rettinger, M.: TCCON data from Garmisch, Germany, Release GGG2014R0, TCCON data archive, Carbon Dioxide Information Analysis Center, Oak Ridge National Laboratory, Oak Ridge, Tennessee, USA, https://doi.org/10.14291/tccon.ggg2014.garmisch01.R0/1149299, 2014.

Sweeney, C., Karion, A., Wolter, S., Newberger, T., Guenther, D., Higgs, J. A., Andrews, A. E., Lang, P. M., Neff, D., Dlugokencky, E., Miller, J. B., Montzka, S. A., Miller, B. R., Masarie, K. A., Biraud, S. C., Novelli, P. C., Crotwell, M., Crotwell, A. M., Thoning, K., and Tans, P. P.: Seasonal climatology of CO_2 across North America from aircraft measurements in the NOAA/ESRL Global Greenhouse Gas Refernce Network, J. Geophys. Res.-Atmos., 120, 5155–5190, https://doi.org/10.1002/2014JD022591, 2015.

Takagi, H., Houweling, S., Andres, R. J., Belikov, D., Bril, A., Boesch, H., Butz, A., Guerlet, S., Hasekamp, O., Maksyutov, S., Morino, I., Oda, T., O'Dell, C. W., Oshchepkov, S., Parker, R., Saito, M., Uchino, O., Yokota, T., Yoshida, Y., and Valsala, V.: Influence of differences in current GOSAT XCO_2 retrievals on surface flux estimation, Geophys. Res. Lett., 41, 2598–2605, https://doi.org/10.1002/2013GL059174, 2014.

Takahashi, T., Sutherland, S. C., Wanninkhof, R., Sweeney, C., Feely, R. A., Chipman, D. W., Hales, B., Friederich, G., Chavez, F., Sabine, C., Watson, A., Bakker, D. C. E., Schuster, U., Metz, N., Yoshikawa-Inoue, H., Ishii, M., Midorikawa, T., Nojiri, Y., Körtzinger, A., Steinhoff, T., Hoppema, M., Olafsson, J., Arnarson, T. S., Tilbrook, B., Johannessen, T., Olsen, A., Bellerby, R., Wong, C. S., Delille, B., Bates, N. R., and de Baar, H. J. W.: Climatological mean and decadal change in surface ocean pCO_2, and net sea-air CO_2 flux over the global oceans, Deep-Sea Res. Pt. II, 56, 554–577, 2009.

Tans, P. and Thoning, K.: How we measure background levels of CO_2 on Mauna Loa, available at: https://www.esrl.noaa.gov/gmd/ccgg/about/co2_measurements.pdf (last access: 7 August 2018), 2016.

van der Werf, G. R., Randerson, J. T., Giglio, L., Collatz, G. J., Mu, M., Kasibhatla, P. S., Morton, D. C., DeFries, R. S., Jin, Y., and van Leeuwen, T. T.: Global fire emissions and the contribution of deforestation, savanna, forest, agricultural, and peat fires (1997–2009), Atmos. Chem. Phys., 10, 11707–11735, https://doi.org/10.5194/acp-10-11707-2010, 2010.

Warneke, T., Messerschmidt, J., Notholt, J., Weinzierl, C., Deutscher, N., Petri, C., Grupe, P., Vuillemin, C., Truong, F., Schmidt, M., Ramonet, M., and Parmentier, E.: TCCON data from Orleans, France, Release GGG2014R0, TCCON data archive, Carbon Dioxide Information Analysis Center, Oak Ridge National Laboratory, Oak Ridge, Tennessee, USA, https://doi.org/10.14291/tccon.ggg2014.orleans01.R0/1149276, 2014.

Waugh, D. W. and Hall, T. M.: Age of stratospheric air: Theory, observations, and models, Rev. Geophys., 40, 1010, https://doi.org/10.1029/2000RG000101, 2002.

Wennberg, P. O., Roehl, C., Wunch, D., Toon, G. C., Blavier, J.-F., Washenfelder, R., Keppel-Aleks, G., Allen, N., and Ayers, J.: TCCON data from Park Falls, Wisconsin, USA, Release GGG2014R0, TCCON data archive, Carbon Dioxide Information Analysis Center, Oak Ridge National Laboratory, Oak Ridge, Tennessee, USA, https://doi.org/10.14291/tccon.ggg2014.parkfalls01.R0/1149161, 2014a.

Wennberg, P. O., Wunch, D., Roehl, C., Blavier, J.-F., Toon, G. C., Allen, N., Dowell, P., Teske, K., Martin, C., and Martin, J.: TCCON data from Lamont, Oklahoma, USA, Release GGG2014R0, TCCON data archive, Carbon Dioxide Information Analysis Center, Oak Ridge National Laboratory, Oak Ridge, Tennessee, USA,

https://doi.org/10.14291/tccon.ggg2014.lamont01.R0/1149159, 2014b.

Wilkerson, J. T., Jacobson, M. Z., Malwitz, A., Balasubramanian, S., Wayson, R., Fleming, G., Naiman, A. D., and Lele, S. K.: Analysis of emission data from global commercial aviation: 2004 and 2006, Atmos. Chem. Phys., 10, 6391–6408, https://doi.org/10.5194/acp-10-6391-2010, 2010.

Wofsy, S. C., Team, H. S., Cooperating, M., and Satellite, T.: HIAPER Pole-to-Pole Observations (HIPPO): fine-grained, global-scale measurements of climatically important atmospheric gases and aerosols, Philos. T. R. Soc. A, 369, 2073–2086, https://doi.org/10.1098/rsta.2010.0313, 2011.

Wofsy, S. C., Daube, B. C., Jimenez, R., Kort, E., Pittman, J. V., Park, S., Commane, R., Xiang, B., Santoni, G., Jacob, D., Fisher, J., Pickett-Heaps, C., Wang, H., Wecht, K., Wang, Q.-Q., Stephens, B. B., Shertz, S., Watt, A. S., Romashkin, P., Campos, T., Haggerty, J., Cooper, W. A., Rogers, D., Beaton, S., Hendershot, R., Elkins, J. W., Fahey, D. W., Gao, R. S., Moore, F., Montzka, S. A., Schwarz, J. P., Perring, A. E., Hurst, D., Miller, B. R., Sweeney, C., Oltmans, S., Nance, D., Hintsa, E., Dutton, G., Watts, L. A., Spackman, J. R., Rosenlof, K. H., Ray, E. A., Hall, B., Zondlo, M. A., Diao, M., Keeling, R., Bent, J., Atlas, E. L., Lueb, R., and Mahoney, M. J.: HIPPO Merged 10-second Meteorology, Atmospheric Chemistry, Aerosol Data (R_20121129), Carbon Dioxide Information Analysis Center, Oak Ridge National Laboratory, Oak Ridge, Tennessee, USA, https://doi.org/10.3334/CDIAC/hippo_010 (Release 20121129), 2012.

Wunch, D., Wennberg, P. O., Toon, G. C., Connor, B. J., Fisher, B., Osterman, G. B., Frankenberg, C., Mandrake, L., O'Dell, C., Ahonen, P., Biraud, S. C., Castano, R., Cressie, N., Crisp, D., Deutscher, N. M., Eldering, A., Fisher, M. L., Griffith, D. W. T., Gunson, M., Heikkinen, P., Keppel-Aleks, G., Kyrö, E., Lindenmaier, R., Macatangay, R., Mendonca, J., Messerschmidt, J., Miller, C. E., Morino, I., Notholt, J., Oyafuso, F. A., Rettinger, M., Robinson, J., Roehl, C. M., Salawitch, R. J., Sherlock, V., Strong, K., Sussmann, R., Tanaka, T., Thompson, D. R., Uchino, O., Warneke, T., and Wofsy, S. C.: A method for evaluating bias in global measurements of CO_2 total columns from space, Atmos. Chem. Phys., 11, 12317–12337, https://doi.org/10.5194/acp-11-12317-2011, 2011.

Yevich, R. and Logan, J. A.: An assessment of biofuel use and burning of agricultural waste in the developing world, Global Biogeochem. Cy., 17, 1095–1134, https://doi.org/10.1029/2002gb001952, 2003.